ASSESSMENT OF WATER SUPPLY CONTAMINATION DUE TO UNDERGROUND COAL GASIFICATION

by

Thomas M. Niemczyk
Associate Professor of Chemistry
University of New Mexico

and

Edward A. Walters
Associate Professor of Chemistry
University of New Mexico

TECHNICAL COMPLETION REPORT

Project No. B-061-NMEX

December 1980

New Mexico Water Resources Research Institute

in cooperation with

Department of Chemistry
University of New Mexico

The work upon which this publication is based was supported in part by funds provided through the New Mexico Water Resources Research Institute by the U.S. Department of the Interior, Office of Water Research and Technology, as authorized under the Water Research and Development Act of 1978, P.L. 95-467, under project No. B-061-NMEX; by the State of New Mexico through the Energy Resource and Development Division of the Energy and Minerals Department; and by the State of New Mexico through State appropriations, under project Nos. 1345641 and 1423641.

The purpose of WRRI technical reports is to provide a timely outlet for research results obtained on projects supported in whole or in part by the Institute. Through these reports, we are promoting the free exchange of information and ideas and hope to stimulate thoughtful discussion and action which may lead to resolution of water problems. The WRRI, through peer review of draft reports, attempts to substantiate the accuracy of information contained in its reports; but the views expressed are those of the author(s) and do not necessarily reflect those of the WRRI or its reviewers.

Contents of this publication do not necessarily reflect the views and policies of the United States Department of the Interior, Office of Water Research and Technology, nor does mention of trade names or commercial products constitute their endorsement or recommendation for use by the United States Government.

Assessment of Water Supply Contamination Due to Underground Coal Gasification

Final Report

By

Thomas M. Niemczyk and Edward A. Walters

Department of Chemistry
University of New Mexico
Albuquerque, NM 87131

Abstract

A site has been chosen in northwestern New Mexico for a proposed underground coal gasification zone and the groundwater. There is no major aquifer in the region of the Fruitland Formation subbituminous coal seam (∿500 ft.), although the zone is saturated and a transmissivity of 0.6 $feet^2 day^{-1}$ has been determined. The groundwater is of poor quality having a pH ≈ 10, conductivity ≈ 6 mmho, total dissolved solids ≈ 3900 ppm, alkalinity ≈ 1700 ppm $CaCO_3$, and hardness ≈ 50 ppm. Na, K, Mg, Ca are the major metal contaminants with environmentally significant ions present on the ppb level (As, Pb, Cd, Be, Cu, etc.). The major anionic species are Cl^-, F^-, SO_3^{2-}, S^{2-}, and HCO_3^-. Deep water samples effervesce when brought to the surface, smelling strongly of H_2S. X-ray diffraction and petrographic examinations of the overburden, parting, and underburden indicate the major minerals to be quartz, feldspars, kaolinite, and montmorillonite. The sediment is fine grained, horizontally stratified, and fractured with fracture filling by calcite and/or gypsum; it also contains a large amount of organic matter. Major and trace element analyses of the sediment finds, aside from Si and Al, Na, Mg, K, Ca, and Fe as the major constituents of this material. The baseline results for the major and trace metal analyses of the groundwater and mineral material, anionic analyses of the groundwater, and trace organic analyses of the groundwater is discussed. A brief description of the local environment is given.

Key words: Underground Coal Gasification, Ion Exchange, Leaching, Groundwater Analysis

Research Project Objectives

The objectives of the research project are as follows:

1. Choose a site in northwestern New Mexico typical of a site where underground coal gasification might be carried out.

2. Drill wells into coal seams saving the core samples for later analysis.

3. Establish the flow patterns of the groundwater in the area by performing hydrology studies.

4. Characterize the soil rock and coal samples obtained in the drilling operation for mineral content as well as trace metal content.

5. Establish a water sampling procedure and obtain water samples from the wells.

6. Perform laboratory analysis of the water samples to establish baseline concentrations of organics, metals, and ionic species.

7. Determine the anions, cations and organics that might be introduced into the water supply by the UCG process.

8. Determine distributions coefficients for the ion exchange processes between ions in solution and the ion exchange sites on the local clays and coals.

9. Determine which ions and organics will be leached from the coal, soil, char, or ash that would be present at the UCG site.

10. Develop a model to describe the movement of species in the groundwater system.

The WRRI funded portion of the work concerns the part of the project designed to establish baseline concentrations of species in the groundwater. Some of the operations such as the drilling and coring are necessarily related to this.

TABLE OF CONTENTS

LIST OF FIGURES

LIST OF TABLES

LIST OF TABLES (Continued)

1. Introduction

This project addresses the question of the potential for pollution by metal ions of groundwater as a consequence of underground coal gasification. The study focuses on subbituminous coal of the San Juan Basin of New Mexico. This section constitutes a report of activities on this grant for the period October 1, 1978-September 30, 1979. Additional financial support was provided by the Energy and Minerals Department of the State of New Mexico through the New Mexico Energy Institute at Socorro, NM and by the Environmental Protection Agency through the Industrial Environment Research Laboratory, Cincinnati, OH.

This project is a critical component of a joint effort between the University of New Mexico, the Public Service Company of New Mexico, and Los Alamos Scientific Laboratory (DOE) to evaluate the feasibility of underground coal gasification (UCG) in the San Juan Basin. The combined laboratory and field study has consisted of site selection, drilling and coring, hydrogeology, baseline analyses from field samples, laboratory studies on metal ion adsorption and exchange, and development of analytical methodology. Results of this work are discussed below.

2. Site Selection

A site was selected for the field test on the basis of the following criteria:

a) The site should contain a seam of subbituminous, noncaking coal.

b) The principal coal seam should be at least 10 feet thick located at least 250 feet below the surface. The seam should have a dip of less than 5 to 10 percent.

c) In order to facilitate obtaining permits, the site should be located on State of New Mexico land.

d) There should be reasonable access to the site via existing roads.

e) The site should be located near existing or future power plant sites.

f) The site should be within reasonable distance of power and water utilities.

A site satisfying these criteria was selected. It is located in the SW 1/4 NW 1/2 of Section 36, Township 30 N, Range 15 W, New Mexico. The site is about 10 miles northwest of Farmington, NM; it is about 3 miles north of State Highway 550 and about the same distance east of the San Juan Generating Station which is owned primarily by the Public Service Company of New Mexico. The site is on State of New Mexico land which is under lease to the Western Coal Company, a partially owned subsidiary of the Public Service Company of New Mexico. Fruitland Formation subbituminous coal lies at a depth of 500 feet at this point in a seam that is 16 feet thick. Fruitland Formation coal was deposited in cretaceous time and is presently located at depths of up to 3000 feet. Those areas in which the coal lies about 250 feet are shown in Figure 1.

The Fruitland Formation is the coalbearing member of interest. It has a thickness of 200 to 300 ft and is composed of a complex interbedding of sandstone, siltstone, shale, carbonaceous shale, carbonaceous sandstone, coal, and (in the lower part) thin limestone beds made up almost entirely of shells of brackish water pelecypods. The thicker coal seams are found in the lower one-third of the formation. In the area of the UCG site the Fruitland Formation coal consists of a single basal bed with a maximum thickness of about 19 feet. The bed is composed of a series imbricate lenses separated by silty, sandy bentonitic partings. This coal was deposited primarily in a paludal (swamp) environment. Such coastal-swamp deposits are characterized by a predominance of organic-rich muds and silts with variable concentrations of nearly pure organic matter. The sections nearest the shoreline are strictly nonmarine even

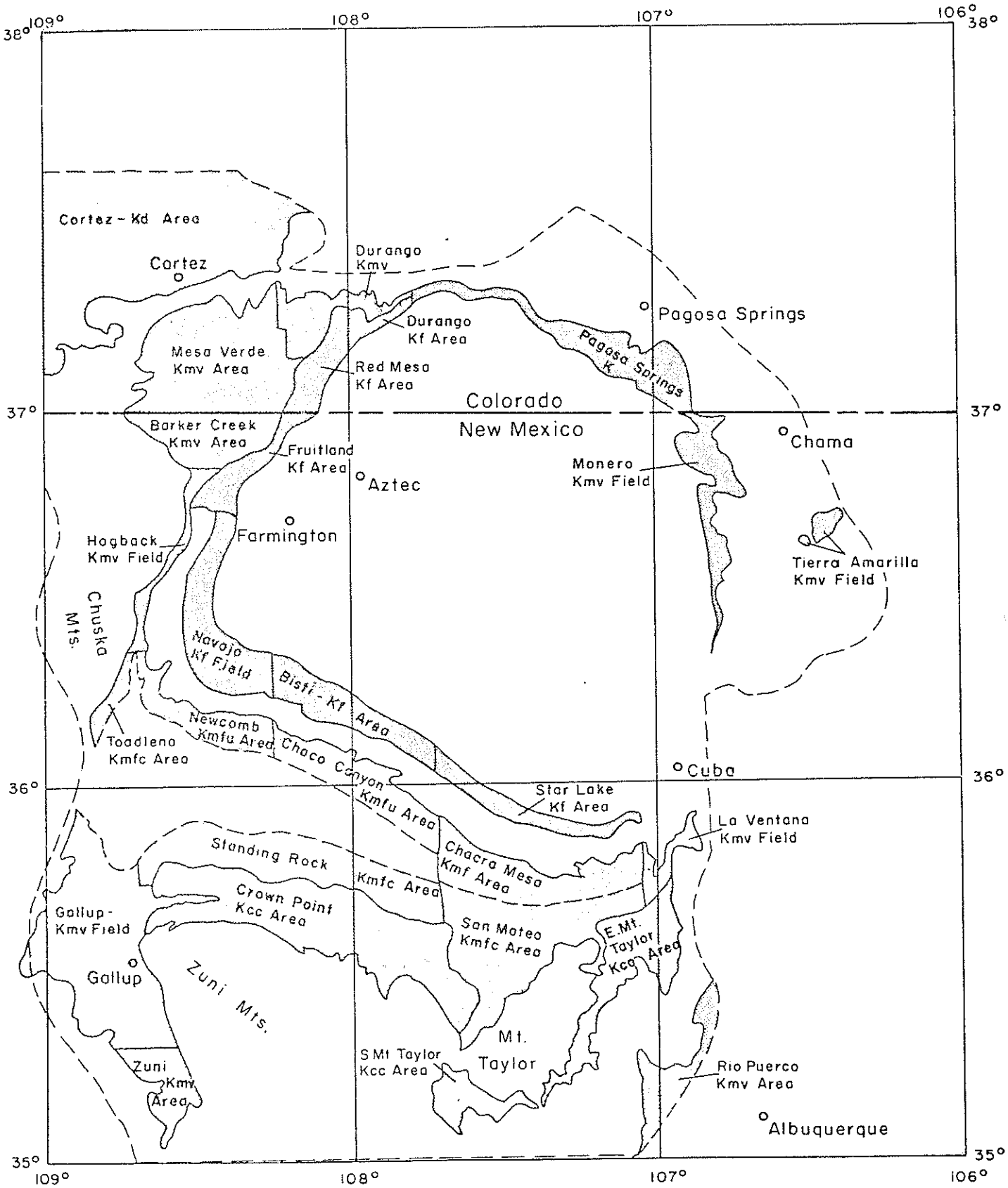

Figure 1. Fields and areas of strippable low-sulfur coal in San Juan Basin.

though they were probably inundated by sea water during storms and under normal conditions the water was likely somewhat brackish.

The Fruitland Formation is overlain by the Kirtland shale which was deposited on the Fruitland Formation through continental erosion. It consists principally of shale, but it also contains soft sandstone and siltstone beds in irregular abundances.

The site is located in arid country which has an annual rainfall of 4-6 inches. The immediate area is drained by the San Juan River which runs northwestward into Utah. It eventually joins the Colorado River. The overall climate is moderate in terms of temperature (average temperature at Fruitland, elevation 5,120 feet, for July is 74°F and for January is 30°F) and arid to semiarid in terms of moisture.

The terrain consists of rolling, sandy hills, nearly devoid of vegetation. At a distance of approximately 1 mile to the north a set of brown sandstone bluffs are found. The surface at the site is within a major erosional area containing largely alkaline soils. Animal densities are very low due to sparse vegetative cover. These features are evident in the 8"x10" black and white photographs and in the color slides taken at the site and submitted to NMWRRI earlier. Figures 2-10 are selected photographs from this series which show the site, its local environment, and some of our sampling activities.

It should be pointed out that the study area is centrally located in the northwest New Mexico energy production complex. Two coal mines and over 2000 MW generating capacity are located within 15 miles of the lease. A 345 kV transmission corridor passes through the property and a natural gas cleaning plant is only about two miles away. A natural gas pipeline crosses the eastern extension of the property.

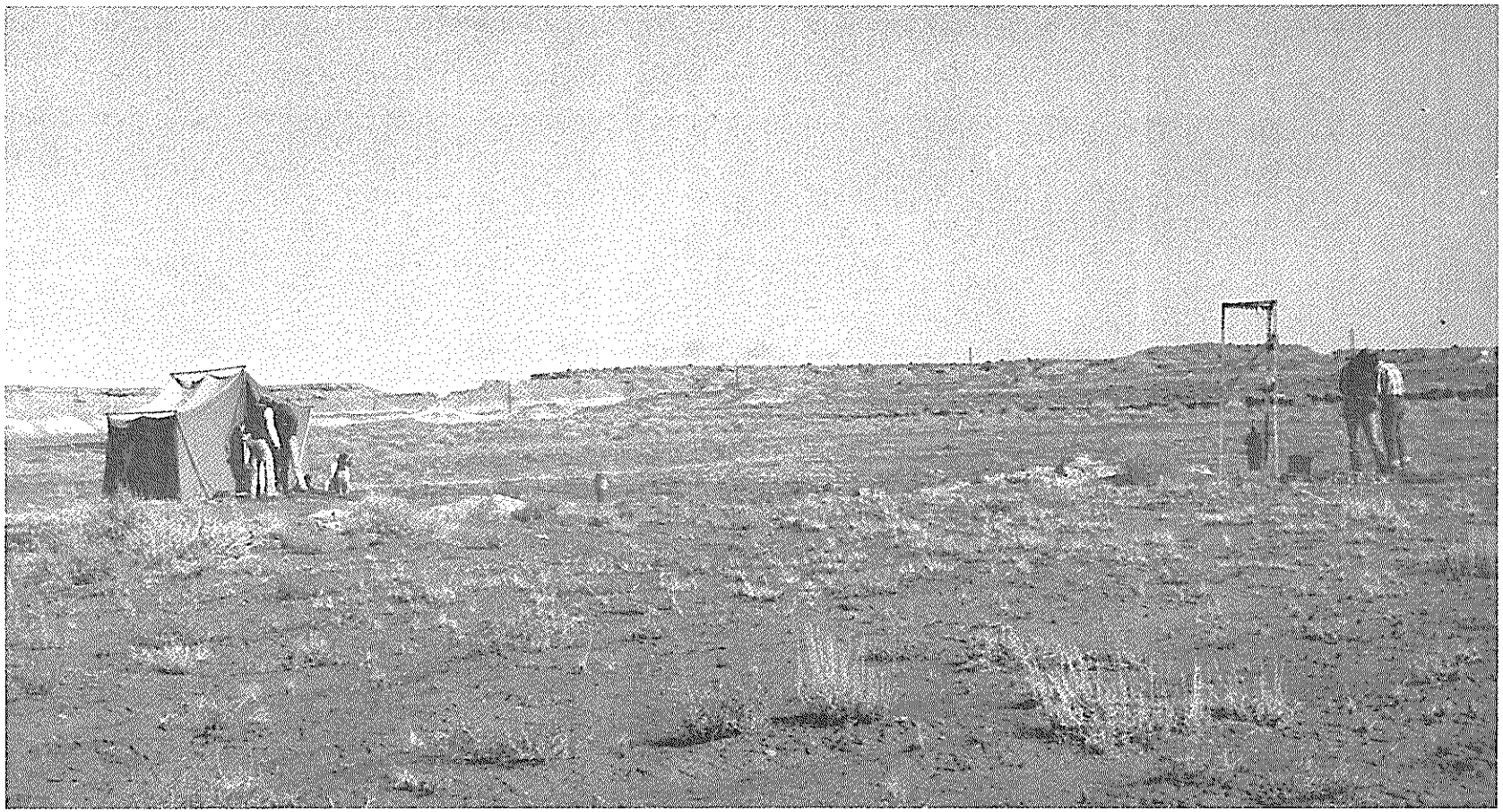

Figure 2. This is a northeasterly view across the UCG site. Both cased wellheads are visible in this photograph. The one just to the left of center is GT-1 and the well underneath the metal framework on the right is the large diameter well, GT-2. The tent serves as the field laboratory. This and the following photographs were taken on February 17, 1979; at this time the site was rather wet due to the recent rains. The mesas in the background are characteristic of this region. The sparseness of the vegetation is evident in the foreground.

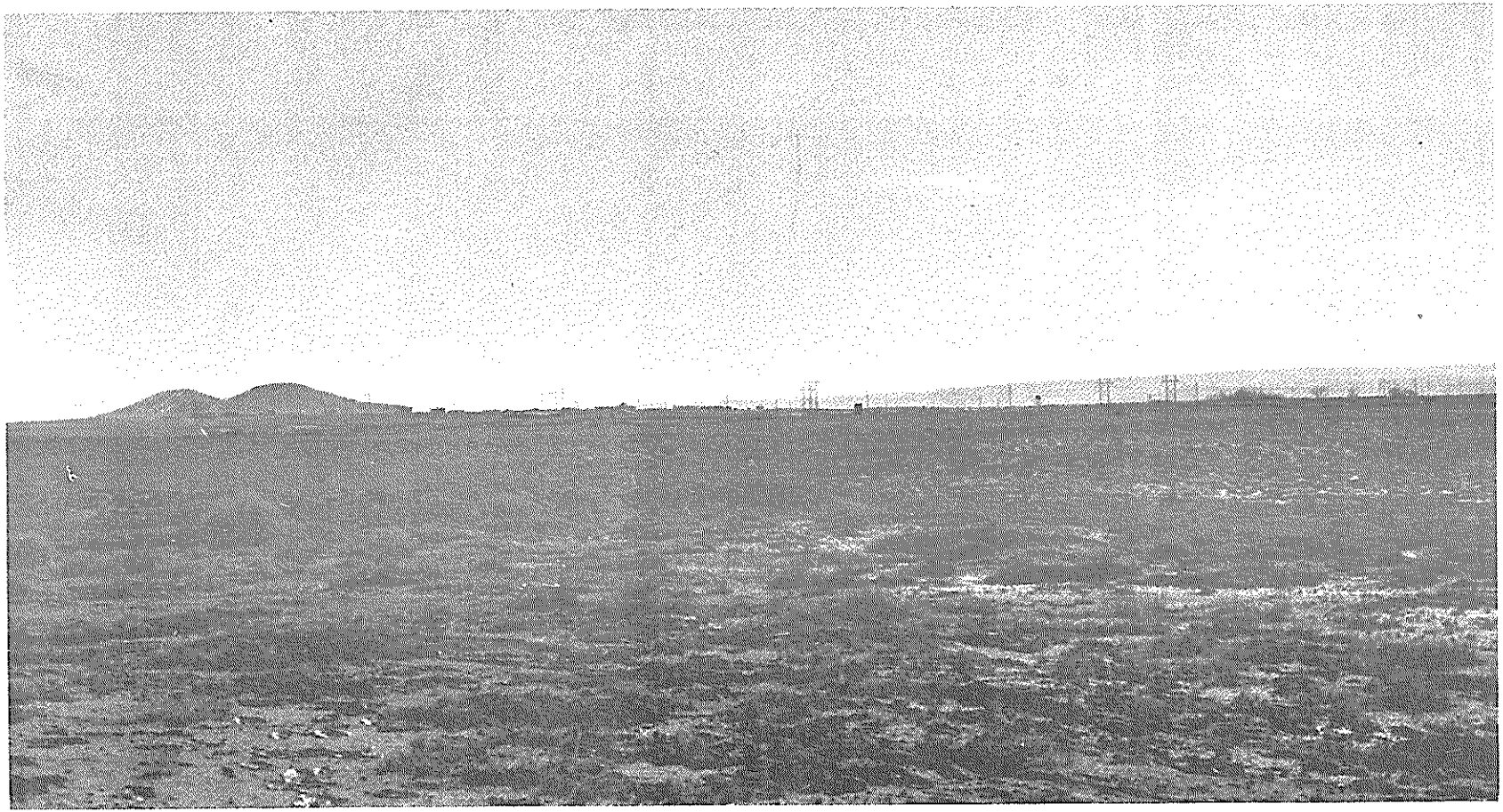

Figure 3. This is a southeasterly view; Farmington is located just to the left of the two hills at the left edge of the photograph. The high voltage power lines come from the San Juan Generating Plant to the west of the site (see later figures). The San Juan River flows from left to right across the photograph and it is located at the near base of the mesas on the horizon in the right side of the picture.

Figure 4. A southerly view with well GT-2 on the right edge of the photograph. Two ice-covered drilling mud pits are in the foreground. The facility at the left is a natural gas cleaning plant operated by El Paso Natural Gas Company. The hill on the right is known as Flare Hill because of the flare tower on it which is no longer in use. The high voltage transmission lines can be seen in this photograph as well.

Figure 5. This is a close-up photograph, taken with a 135 mm telephoto lens, of the natural gas cleaning plant. The access road can be seen at the left. It has just been graded to make it passable after the recent rains.

Figure 6. This is a northwesterly view across the site with both wells visible; the field laboratory, the drilling mud pits and the San Juan Generating Plant are also apparent.

Figure 7. This is a telephoto view (135 mm lens) of the San Juan Generating Plant taken from the same location as Figure 6. This photograph views the generating plant across the strip mine operated by Western Coal Company which supplies coal to the San Juan Plant. The boom of the dragline can be seen through the uprights of the third set of transmission line towers from the left. Note the uniformly low density of vegetation in the entire region.

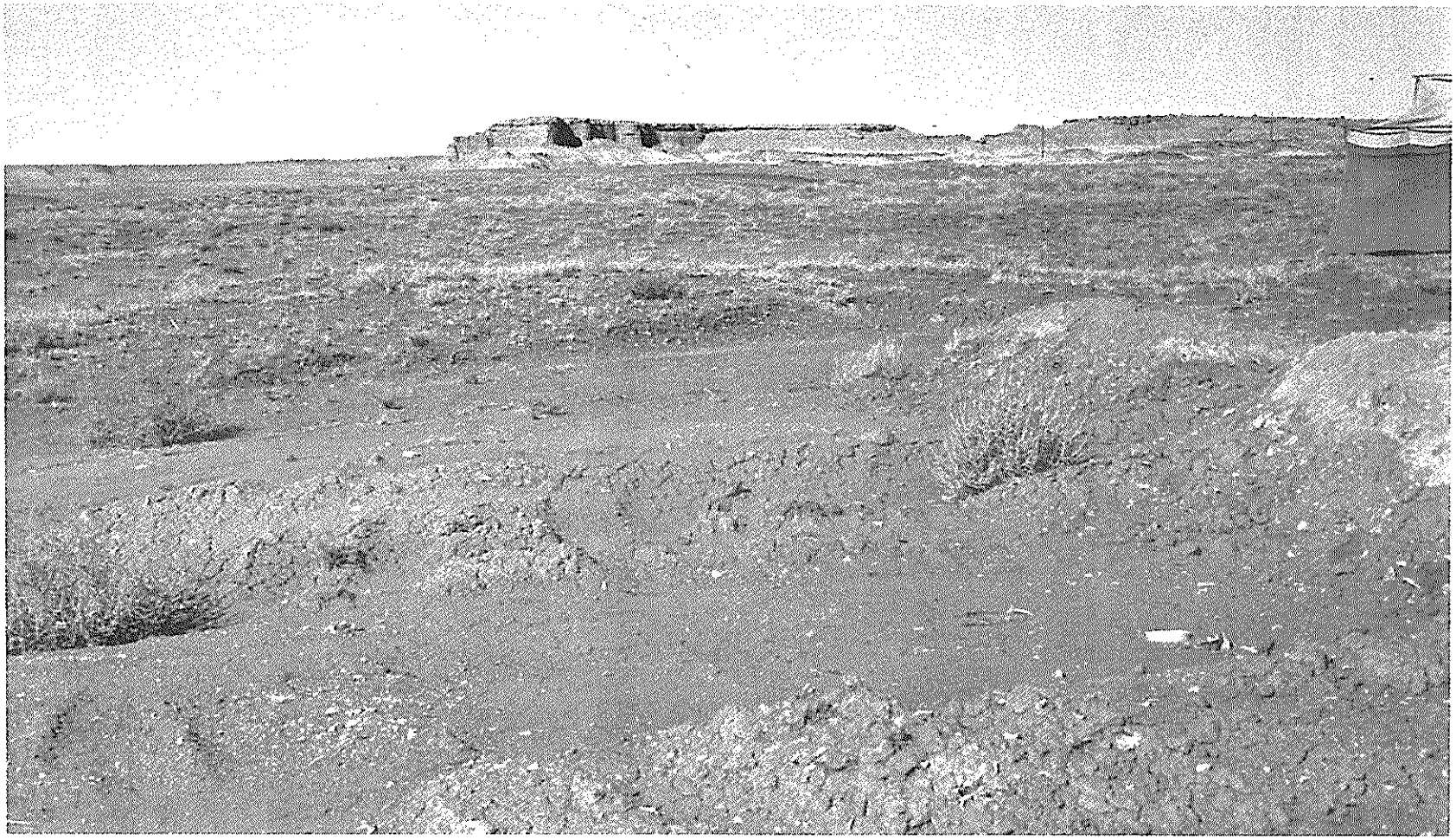

Figure 8. This is a northerly view from the UCG site. The field laboratory tent can be seen on the right. The surface in the foreground was scarred during drilling operations.

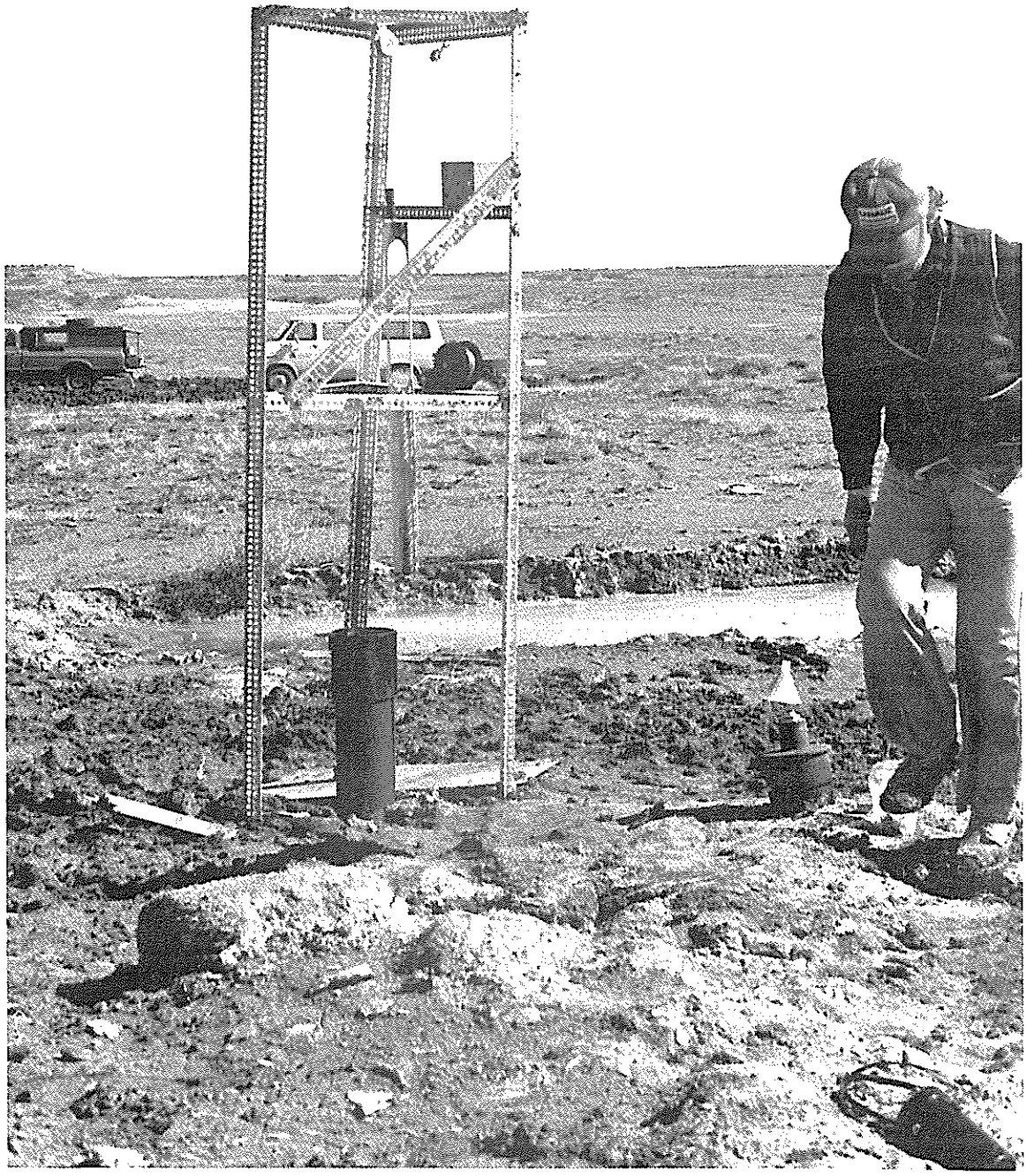

Figure 9. The sampling system in position above GT-2. The sampler hangs above the well just after being brought up with a sample of about 1500 ml of deep water.

Figure 10. A closeup of the sampler at the wellhead of GT-2. The winch used for lowering and raising the sampler is located in the upper right-hand corner of the photograph.

3. Drilling and Coring

A two-hole pattern of wells has been drilled into the Fruitland Formation at the selected UCG test site. Surveyed coordinates of the two wells are:

Well No.	N. Coord.	E. Coord.	Elevation
GT-1	2,100,399.4 ft. 640,203.02 m	342,253.6 ft. 104,319.11 m	5297.3 ft 1614.62 m
GT-2	2,100,402.7 ft. 640,204.02 m	342,283.8 ft. 104,328.31 m	5296.9 ft. 1614.50 m

The wells were drilled, cored, completed and cased in April, 1978 using funds provided by the Public Service Company of New Mexico. Special care was taken to assure vertical drilling at both holes. Subsequent experience indicates that the wells are in fact very nearly vertical. A chronological log of drilling and completion of the wells is given in Table I. Cores were taken from both wells (GT-1, 4-inch id, and GT-2, 6-inch id) from about 15 feet above the principal seam to about 15 feet into the Pictured Cliffs sandstone which makes up the underburden. Descriptions of the cores from GT-1 and GT-2 are reported in Tables II and III, respectively. Casings were set to just above the coal and cemented in place. It is interesting to note that the coal in GT-2 is encountered at a depth of about 2 m (6 ft) greater than in GT-1. This is a consequence of the overlapping lenticular shapes of the individual deposits of organic matter which later coalified. In fact, in GT-1 a silty stringer is observed at the depth where coal begins in GT-2 suggesting that in the short distance between the wells, 10 m (30 ft), the upper lens seen in GT-1 has essentially disappeared and only the thicker portion of the lower lens is seen in GT-2.

Table I. Chronological description of the drilling and well completion for holes GT-1 and GT-2.

GT-1		
4/4/78	0-300 Drilled	4-3/4 in.
4/5/78	300-480 Drilled	4-3/4 in.
4/6/78	480-484 Cored	Nx split tube 10 ft. core barrel
4/6/78	484-522 Cored	"
4/7/78	522-532 Cored	"
4/7/78	480-532 Reamed	4-3/4 in.
4/12/78	0-501 Reamed	5-5/8 in.
4/13/78	0-501 Wash Out Hole	
4/13/78	Geophysical Logging by Century Geophysical of Grants	
4/14/78	0-496 Set Casing and Cemented	4-1/2 in. OD L/S pipe 20 ft. section welded
4/17/78	0-496 Drill Out Cement in Pipe Wash Out Hole Bailing Test	
GT-2		
4/7/78	0-300 Drilled	4-3/4 in.
4/8/78	300-470 Drilled	4-3/4 in.
4/10/78	470-495.2 Cored	Nx split tube 10 ft core barrel.
4/11/78	495.2-518.2 Cored	"
4/11/78	Western Coal Co. Logging Only	
4/13/78	517.6-522.6 Cored	"
4/13/78	Geophysical Logging by Century Geophysical of Grants	
4/15/78	0-360 Reamed	7-7/8 in.
4/17/78	360-501 Reamed	7-7/8 in.
4/17/78	0-501 Set Casing & Cemented	6-5/8 OD L/S pipe 20 ft. section welded
4/20/78	0-501 Drill Out Cement in Pipe Wash Out Hole Bailing Test	

Table II. Core description versus depth for GT-1.

GT-1

From (ft.)	To	Material
480.0	483.6	shiny gray, hard
483.6	484.0	core loss
484.0	492.4	shiny gray, hard, sandy bottom, 1.2 ft
492.4	492.5	core loss
492.5	495.8	shiny gray, hard, silty
495.8	498.95	coal, medium bright, hard, fractured, resinous
498.95	499.25	shiny, black, carbonaceous
499.25	499.85	coal, dull, hard, very shaley
499.85	500.80	shiny black, hard
500.80	502.5	coal, dull, fractured
502.5	504.2	coal, medium bright, hard
504.2	504.7	shiny black, carbonaceous, sandy at top; coal, medium bright, hard
506.4	506.8	shiny black, hard, carbonaceous, light tan silty band 0.02 at bottom and 0.10 from top, mixed with coal
506.8	511.2	coal, medium bright, hard, resinous
511.2	511.3	shiny, light tan, hard
511.3	512.5	coal, medium bright, hard, resinous
512.5	517.2	coal, medium bright-bright, hard, resinous
517.2	518.3	shiny gray, hard
518.3	522.0	siltstone, gray, very hard, interbedded with thin SS lenses

Table III. Core description versus depth for GT-2.

GT-2

From (ft.)	To	Material
470	474	shale-gray, hard
474	474.5	shale-gray, hard with sandstone veins
474.5	476.0	shale-gray, hard with coal inclusions
476.0	480.0	core loss
480	486.6	shale, gray, moderately firm, sandy, sandstone stringers, coal inclusions
486.6	488.0	shale gray to dark gray, moderately firm to firm
488.0	490.0	shale gray to dark gray, moderately firm to firm
490.0	491.0	shale gray to dark gray, hard, fine to medium grained, stringer of coal at 491.0)
491.0	493.5	sandstone-light gray, hard, fine to medium grained, carbonaceous stringers
493.5	494.7	core loss
494.7	496.0	shale, gray, moderately firm to firm, somewhat sandy
496.0	501.7	shale-gray to dark gray, firm to very firm, somewhat sandy, carbonaceous inclusions
501.7	502.6	carbonaceous shale-gray, sandy, sandstone stringers
502.6	502.8	carbonaceous shale-light brown, firm, sandy, highly carbonaceous
502.8	504.0	coal-black, hard, dull, pyrite, resinous (one thin sandstone stringer).
504.0	508.1	coal-black, hard, dull, pyrite on fractures, resinous
508.1	508.7	sandstone-brown, soft, medium to coarse-grained
508.7	510.7	coal-black, hard, dull, pyrite, resinous
510.7	510.9	sandstone-brown to dark brown, fine-grained, firm, carbonaceous
510.9	514.0	coal-black, dull, hard, pyrite with resin
514.0	515.8	coal-black-dull, hard and brittle, pyrite and resinous
515.8	517.1	carbonaceous shale-dark brown (inclusions of coal) highly carbonaceous
517.1	518.2	shale, gray, firm, sandy
518.2	519.0	core loss

4. Hydrology

The hydrology of the San Juan Basin is the subject of a long term project by the U.S. Geological Survey (1). The results of significance to this study are that in the vicinity of the UCG site water is found in the Kirtland shale and typically fills wells to within 130 ft. of the surface. It is believed that this water is effectively part of a confined aquifer which very slowly drains in the direction of the San Juan River actually entering the river well downstream through springs and seeps. The aquifer does not refill from the surface, but from exposed sections of Kirtland shale and Fruitland Formation coal at nearby mesas.

Shortly after the wells were drilled a set of draw-down tests were conducted by the USGS. These consisted of slug-type tests in which 26-28 gallons of water were removed from GT-2 with a PVC bailer 4 inches in diameter and 4.3 feet long. After bailing, water recovery rates were determined by measuring the water level at frequent intervals. The raw height-time data were treated by the standard procedure for confined aquifers (2). From this a transmissivity of 0.6 $ft^2 day^{-1}$, a permeability of the shale of 0.01 mdarcies, and a storage coefficient of 10^{-5} were calculated. These results are in good agreement with 0.01 mdarcies obtained from an independent laboratory determination of the permeability of Kirtland shale. Very low permeabilities ($\sim$0.1 mdarcies) have also been reported for Pictured Cliffs underburden. On the other hand the permeability of the coal is about 10 mdarcies (3). As a consequence, Fruitland Formation coal is water-saturated and lies well below the water table. The water migration rate appears to be 1-2 ft. $yr.^{-1}$, so that little flow occurs through the UCG site. Thus, the seams must be dewatered prior to gasification, but it seems that there will be no problem of excessive water. This flow rate also suggests that equilibrium will be established between dissolved ions in the water and any adsorption or

ion exchange sites in the rock, clay, or coal. This is a very important conclusion for application of laboratory studies of adsorption and for simulations.

During July, 1979 more extensive tracer studies will be performed at the UCG site to determine detailed permeability and porosity characteristics of the coal seam itself. These studies are being supported by a grant from the DOE and include participation by Los Alamos Scientific Laboratory. The results of the hydrology, and other, studies have been summarized in a paper that is included as Appendix B.

5. Water Baseline Studies

Preliminary water samples were removed from well GT-1 by bailing techniques by the USGS. Glass containers were used and few precautions were taken to stabilize the samples, so the trace metal, anion and organic analyses are not reliable. These results however (4) indicate that the water is brackish (1000-10,000 ppm TDS) and has characteristics similar to groundwater found elsewhere in the Southwest (5).

Deep sampling devices have been built (6), Figure 11, and have been used to collect samples for baseline studies reported here. This device has an open-ended tube with a plug suspended above it. Water flows through and fills the sampler as it descends. When the appropriate depth is reached the sampler is allowed to stabilize briefly and a stainless steel messenger is dropped down the 140 lb. test braided nylon support line; this triggers closure of the device. The filled sampler is retrieved by means of a hand-operated winch and the sample is transferred to a large plastic beaker. The sampler collects about 1400 ml at a time. Measurements of temperature, specific conductivity and pH were made on each sample immediately after collection. The sample is then filtered and the appropriate preservation procedures were followed. The preserved samples were kept cold in plastic bottles until analyses were performed in the laboratory.

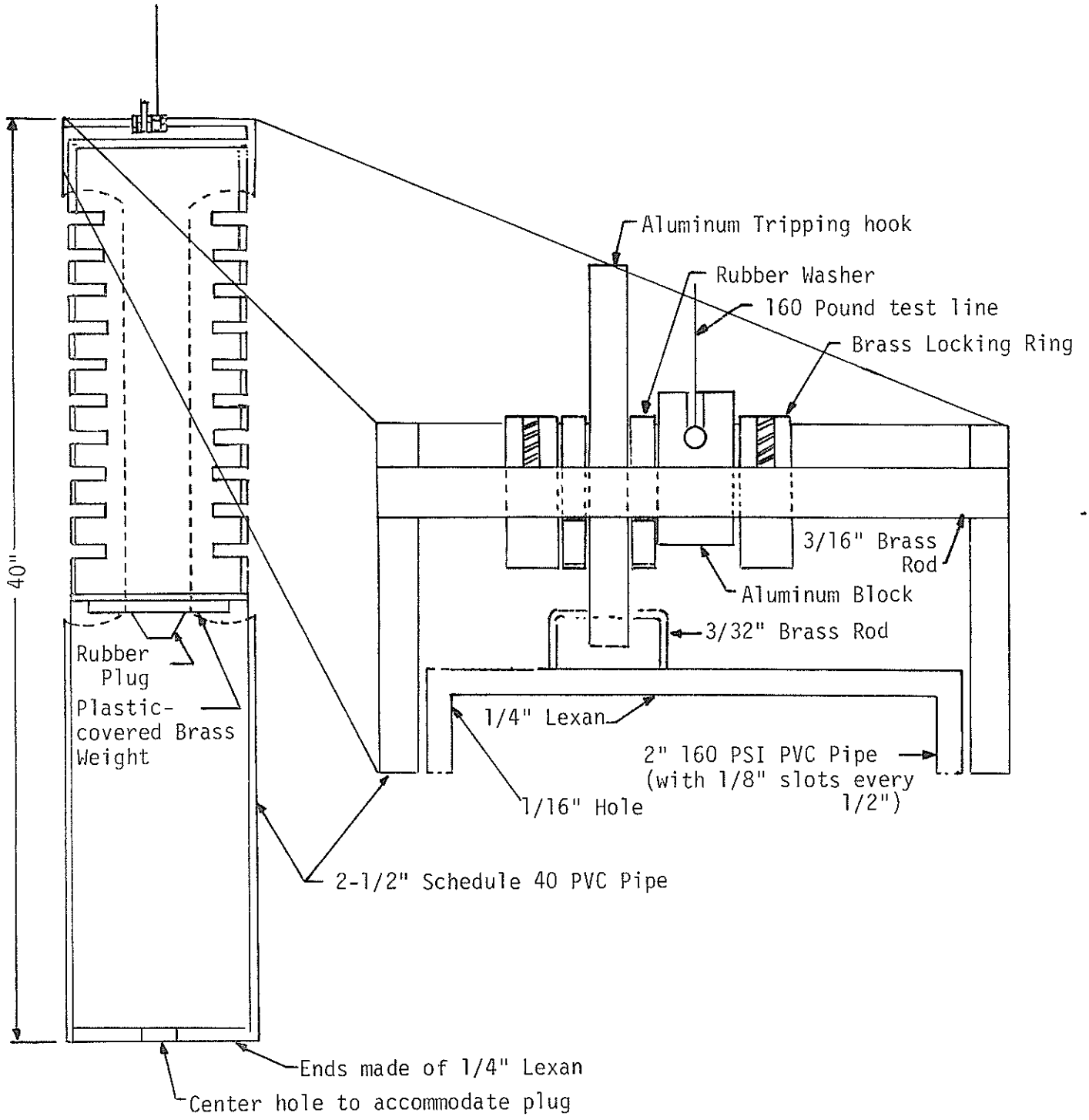

Figure 11. In-situ sampling device.

The position of the sampler in the well was determined by passing the support line around a wheel which was connected to a revolutions counter. The device was calibrated and it is believed that the reported depths are reliable to within 2 feet and that the depth reproducibility is approximately 6 inches.

Filtration turned out to be the primary field problem. The source of the problem lies in the fine clay-size particles suspended in the deep water samples. Clays make up a large fraction, as high as 60%, of the overburden, so the samples were badly contaminated with clays. Initially a standard millipore filtering apparatus with 47 mm diameter filters, 0.45 μm pore size, was used to filter the samples. Restricting the vacuum in the receiving flask to no less than 15 mm Hg, approximately 10 minutes were required to filter 100 ml of sample. At this point the filter was clogged and had to be changed. Consultation with Lepp at the USGS (7) led to a satisfactory solution to this problem. A filter plate of acrylic plastic was made which receives 147 mm diameter filters. Once again the filters have a pore size of 0.45 μm. The filter is placed between two sheets of nylon screen and positioned over the bottom plate. This plate has a series of grooves machined in it to permit uniform drainage of the filter. The filtrate is collected from a drain in the center of this plate. The top plate has a set of grooves matching those on the lower plate. This is clamped over the filter and the mixture to be filtered is driven through the system by means of a peristaltic pump. The pump operates on an input voltage of 12 volts, so an automobile battery can be used as a power supply for field work. An additional advantage to this device is that the pump can be reversed briefly to backflush the filter. This serves to open clogged pores so more mixture can be filtered. With this apparatus filtration problems were minimized.

Standard methods (8-10) were used for analyses of the samples. Field measurements were carried out for pH, conductivity, temperature, chloride, and fluoride. Samples were preserved according to EPA approved procedures and transported to the University of New Mexico in Albuquerque for subsequent analysis. A Varian AA6 was used for all atomic absorption measurements. This instrument was purchased for this project by funds provided by the Energy and Minerals Department of the State of New Mexico through the New Mexico Energy Institute at Sorocco.

The dates of sample collection and the wells sampled during 1979 are given in Table IV. Samples were collected both in the overburden region below the

Table IV. Dates of sample collection and wells sampled during 1979.

Date	Wells sampled
January 12	GT-2
February 17	GT-1, GT-2
April 30	GT-1
May 1	GT-2

casing and in the region of the coal seam. The wells had both been partially filled by detritus from sloughing of the sides below the casing, so it was not possible to collect samples in the underburden levels.

To this date baseline water samples have been acquired from the two wells and analyzed. The intention is to compare these results with those from water samples collected after a burn between the two wells. The concentrations observed for the species we intend to monitor are collected in Table V.

As anticipated, the principal cations are Na^{+}, K^{+}, Ca^{+2}, and Mg^{+2}, the majority anions are Cl^{-}, $SO_4^{=}$, and HCO_3^{-}. These seven species account for essentially all of the mass observed in the total dissolved solid analyses.

Table V. Baseline results of water samples collected from wells GT-1 and GT-2.

Analysis	Units	GT-1		GT-2	
		2/17/79	4/30/79	2/17/79	5/1/79
Cu^{+2}	µg/ℓ	53	3.6	--	1.5
Zn^{+2}	µg/ℓ	14	10.4	--	10.5
Pb^{+2}	µg/ℓ	50	--	--	--
Na^{+}	mg/ℓ	1380	1100	--	1045
K^{+}	mg/ℓ	14.5	8.8	--	6.06
Ca^{+2}	mg/ℓ	1.3	1.7	--	1.9
Mg^{+2}	mg/ℓ	0.42	0.30	--	2.05
Sr^{+2}	mg/ℓ	0.2	0.35	--	0.45
Cd^{+2}	µg/ℓ	14	<0.7	--	0.6
Ni^{+2}	µg/ℓ	<0.7	<2	--	<3
Co^{+3}	µg/ℓ	20	<2	--	<3
Cr^{+3}	µg/ℓ	0	<7	--	<7
Sn^{+4}	mg/ℓ	<0.4	--	--	--
Fe^{+3}	mg/ℓ	--	1.05	--	0.108
Cl^{-}	mg/ℓ	--	1170	1150	1325
$SO_4^{=}$	mg/ℓ	--	132	813	24.5
$S^{=}$	mg/ℓ	--	4.38	25.4	0.175
F^{-}	mg/ℓ	--	2.25	2.55	2.60
$PO_4^{\equiv}$ as P	mg/ℓ	--	0.10	0.238	0.076
CN^{-}	µg/ℓ	--	3.4	7.81	2.5
NO_3^{-} qs N	µg/ℓ	--	<10	<10	<10
NO_2^{-} as N	µg/ℓ	--	<2	<2	<2
NH_4^{+} as N	mg/ℓ	--	10.30	--	2.30
Alkalinity	mg/ℓ	--	1203	1712	1710
TDS	mg/ℓ	--	4164	3902	3899
CoD	mg/ℓ		<15	<15	<15
pH		9.25[a]	10.66[a]	7.82[a]	9.65[a]
			10.48[b]	8.17[b]	9.64[b]
Water temperature	°C	15.5[a]	19.7[a]	15.6[b]	19.0
			18.9[b]	18.9[b]	19.9[b]
Specific conductance	mmho/cm	4.85[a]	6.39[a]	4.60[a]	5.53[a]
			6.20[b]	4.78[b]	5.73[b]

a) Sample taken at the overburden level.
b) Sample taken at the coal seam level.

There are several rather glaring inconsistencies in these results, most notably the variation in $SO_4^=$ concentrations. We offer no explanation for these changes at the present time; it is expected that further sampling will clarify the results. The possibility that a sulfate-reducing bacterium such as Desulfouibrio desulfuricans was introduced has not been discounted. It is interesting that although the two wells are only 30 feet apart the pH differs by 1 full unit and there appear to be real differences in the chemical composition of the water. As indicated earlier, this water falls into the brackish category and has contaminant levels comparable to brackish water collected elsewhere in the Southwest.

The samples were not analyzed for H_2S although it is clear that a substantial amount is present. When samples are withdrawn from the well they effervesce. The strong odor of H_2S indicates that some of the gas is H_2S, but it is possible that other dissolved gases such as CH_4 are present also. Samples of the well gases have been collected, but their analysis is not yet complete.

A comparison of these data with similar results from two other UCG sites is useful. Campbell, Pellizzari, and Santor (11) have examined groundwater prior to an following a UCG test at the Hoe Creek site in Wyoming. At this site the pregasification water was much less highly contaminated and exhibited a relatively low pH of 7.5. The same chemical species dominate the solution. After the burn the pH, TDS, and conductivity increased to values similar to our baseline results. Colchin, Turk and Humenick (12) have conducted an extensive set of groundwater sampling experiments in aquifers contained in lignite coals in Texas. The baseline results in this case also show the groundwater is much cleaner than San Juan basin groundwater. The water is also much more nearly at neutral pH and the conductance is correspondingly lower.

6. Coal Baseline Studies

The core from GT-1, 2-1/8-inch diameter, was sliced in half lengthwise with a diamond saw at the request of Western Coal Company. Half of the core was used for immediate analysis and study and half was reserved for later use. The working half was separated into 6-inch segments, ground to -60 mesh, sieved, and sealed in screw-top glass laboratory containers for subsequent analysis. An index to the samples is given in Table VI. Proximate and heating value analyses were performed on alternate samples over the coal bearing portions of this core. Data normalized to water-free conditions are given in Table VII. Included in these analyses was a parting at a depth of about 500 ft. It's location is identified by the high ash content of samples 39-49.

The results are typical of Fruitland Formation coal; although the heating values are high enough formally to qualify it for a bituminous coal rank, both the percent of fixed carbon and the nonagglomerating characteristics identify it as subbituminous A or B coal. There is a substantial amount of ash present, the maximum clearly falling at the location of the parting. The amount of sulfur in the coal is characteristic of San Juan basin coal, lying in the range of 0.50 - 0.80%.

Studies on trace metal characterization of the coal have been initiated. In one experiment both raw and treated Fruitland Formation coal were fused with lithium metaborate; the product was dissolved in aqueous acid and analyzed for a selection of metals by AA. Treated coal was prepared from raw coal by extraction of organics first with ether, then benzene, and finally methanol. As an indication of the changes induced, the raw coal had 10% ash while the treated coal had 14% ash. Some problems arose with fusion so the results are not totally reliable. The experiment is being repeated. The results of this first experiment are reported in Table VIII as percent of the metal element in raw and treated coal samples. These values should be taken as minima; the true values

Table VI. Index of samples prepared from the GT-1 core.

Sample No.	Depth Ft.	Sample No.	Depth Ft.	Sample No.	Depth Ft.
1.	480.0-480.5	29.	494.0-494.5	57.	508.0-508.5
2.	480.5-481.0	30.	494.5-495.0	58.	508.5-509.0
3.	481.0-481.5	31.	495.0-495.5	59.	509.0-509.5
4.	481.5-582.0	*32.	495.5-496.0	60.	509.5-510.0
5.	482.0-482.5	33.	496.0-496.5	61.	510.0-510.5
6.	482.5-483.0	34.	496.5-497.0	62.	510.5-511.0
7.	483.0-483.5	35.	497.0-497.5	63.	511.0-511.5
8.	483.5-484.0	36.	497.5-498.0	64.	511.5-512.0
9.	484.0-484.5	37.	498.0-498.5	65.	512.0-512.5
10.	484.5-485.0	38.	498.5-499.0	66.	512.5-513.0
11.	485.0-585.5	39.	499.0-499.5	67.	513.0-513.5
12.	485.5-486.0	40.	499.5-500.0	68.	513.5-514.0
13.	486.0-486.5	41.	500.0-500.5	69.	514.0-514.5
14.	486.5-487.0	42.	500.5-501.0	70.	514.5-515.0
15.	487.0-487.5	43.	501.0-501.5	71.	515.0-515.5
16.	487.5-488.0	44.	501.5-502.0	72.	515.5-516.0
17.	488.0-488.5	45.	502.0-502.5	**73.	516.0-516.5
18.	488.5-489.0	46.	502.5-503.0	74.	516.5-517.0
19.	489.0-489.5	47.	503.0-503.5	75.	517.0-517.5
20.	489.5-490.0	48.	503.5-504.0	76.	517.5-518.0
21.	490.0-490.5	49.	504.0-504.5	77.	518.0-518.5
22.	490.5-491.0	50.	504.5-505.0	78.	518.5-519.0
23.	491.0-491.5	51.	505.0-505.5	79.	519.0-519.5
24.	491.5-492.0	52.	505.5-506.0	80.	519.5-520.0
25.	492.0-492.5	53.	506.0-506.5	81.	520.0-520.5
26.	492.5-493.0	54.	506.5-507.0	82.	520.5-521.0
27.	493.0-493.5	55.	507.0-507.5	83.	521.0-521.5
28.	493.5-494.0	56.	507.5-508.0	84.	521.5-522.0

* Beginning of Coal Seam
** Bottom of Coal Seam

the core extends to 532 ft.

Table VII. Geochemical properties of the GT-1 core versus depth*.

Sample No.	Depth (ft.)	C	H	O	N	S	Ash	Heating Value** Btu/lb.	Volatile	Fixed Carbon
33	496.0-496.5	68.49	5.16	11.73	1.19	0.67	12.76	12252	41.34	45.90
34	496.5-497.0									
35	497.0-497.5	72.07	5.37	11.60	1.72	0.67	8.57	12907	42.62	48.81
36	497.5-498.0									
37	498.0-498.5	71.46	5.18	11.48	1.81	0.71	9.36	12708	42.20	48.44
38	498.5-499.0									
39	499.0-499.5	34.78	2.81	8.62	0.57	1.59	51.62	5899	23.70	24.68
40	499.5-500.0									
41	500.0-500.5	12.97	1.16	5.48	0.39	1.09	78.89	2065	11.15	9.96
42	500.5-501.0									
43	501.0-501.6	55.39	4.30	10.59	1.46	0.94	27.31	9840	36.07	36.62
44	501.5-502.0									
45	502.0-502.5	44.76	3.52	7.99	1.31	2.34	40.08	7962	28.15	31.77
46	502.5-503.0									
47	503.0-503.5	47.72	3.84	9.57	1.33	0.76	36.78	8461	30.40	32.82
48	503.5-504.0									
49	504.0-504.5	39.34	3.30	11.27	1.03	0.83	44.19	6731	27.65	28.16
50	504.5-505.0									
51	505.0-505.5	72.80	5.13	11.34	1.77	0.66	8.30	12777	40.75	50.95
52	505.5-506.0									
53	506.0-506.5	70.98	5.28	10.58	1.72	0.64	10.80	12514	41.11	48.09
54	506.5-507.0									
55	507.0-507.5	62.31	4.66	11.17	1.15	0.56	20.15	10983	37.79	42.06
56	507.5-508.0									
57	508.0-508.5	71.52	5.18	12.34	1.09	0.50	9.37	12672	41.76	48.87
58	508.5-509.0									
59	509.0-509.5	72.37	5.23	11.51	1.56	0.54	8.78	12867	41.83	49.39
60	509.5-510.0									
61	510.0-510.5	72.44	5.54	11.08	1.65	0.57	8.71	12960	43.03	48.26
62	510.5-511.0									
63	511.0-511.5	55.89	4.51	10.71	1.51	0.54	26.84	9939	36.73	36.43
64	511.5-512.0									
65	512.0-512.5	58.11	4.57	10.71	1.54	0.51	24.55	10435	38.70	36.75
66	512.5-513.0									
67	513.0-513.5	46.67	4.00	10.48	1.28	0.44	37.12	8365	33.43	29.45
68	513.5-514.0									
69	514.0-514.5	71.63	5.39	11.05	1.79	0.51	9.63	12807	43.84	46.53
70	514.5-515.0									
71	515.0-515.5	73.76	5.77	10.75	1.88	0.49	7.34	13326	46.34	46.32
72	515.5-516.0									
73	516.0-516.5	71.73	5.44	11.84	1.66	0.59	8.74	12952	42.97	48.29

* moisture free basis
** as received

Table VIII. Percent composition of trace metals in raw and treated Fruitland Formation coal.

Metal	Raw Coal	Treated Coal
Be	0.0	0.001
Na	0.455	0.409
Mg	0.39	0.38
Al	8.00	6.50
Si	4.23	3.23
K	0.50	0.50
Ca	3.1	2.4
V	0.04	0.04
Cr	0.005	0.005
Mn	0.005	0.004
Fe	1.09	0.890
Co	0.0	0.0
Ni	0.0055	0.005
Cu	0.15	0.014
Zn	0.0095	0.0065
Ge	< 0.23	< 0.23
Sr	0.0055	0.043
Mb	< 0.048	< 0.048
Cd	0.0	0.0
Sn	< 0.25	< 0.25
Sb	0.003	0.003
Ba	0.13	0.1
Pb	0.02	0.02
Bi	0.0	0.0

will be somewhat higher. The significant conclusion from this experiment is that most metals may be found in at least trace quantities in San Juan Basin coal. It is interesting to note that these compositions generally parallel the abundances of the respective elements in the earth's crust (13), though there are notable exceptions.

Later fusion experiments were repeated on raw coal and on coal that had been subjected to repeated acid washes of HCl and HF to remove mineral matter. The results are given in Table IX. Acid washing reduced the ash content of the coal from 44.9% to 1%; even though most of the ash was removed by the washings, a small amount remained. This is a significant source of trace metals that interfered with some of the adsorption experiments. It appears that the washing procedure was not as effective in removing iron and calcium as it was in removing most of the other metal ions investigated. These results confirm the fusion data in Table VIII which show that most of the natural elements can be found in coal in at least trace quantities.

A preliminary experiment was performed in which a coal sample was placed in the thimble of a Soxhlet extractor and extracted with water for seven days. The resulting solution was analyzed for a number of metal ions. The results are given in Table X as nanograms of analyte per gram of coal. Anion analyses have not yet been carried out on this sample. The high concentrations of alkali metals is consistent with the baseline water results from wells GT-1 and GT-2. The soluble compounds that were extracted in this experiment are most likely alkali metal chlorides and sulfates. Analysis of this solution for additional metals, anions, TDS, etc., is in progress.

We have experienced some problems with the low temperature ashing device so it has not been possible to do a complete analysis of the minerals in the coal. The main problem was poor design of the induction coil; it was held

Table IX. Comparison of raw coal and acid washed coal compositions (%).

	Raw Coal Ash	Raw Coal[a]	Acid Washed coal ash	Acid Washed[b] coal
Si	19.58	8.79	0.89	0.009
Al	11.56	5.19	8.82	0.088
Na	1.75	0.79	0.46	0.005
K	0.77	0.35	0.52	0.005
Mg	0.72	0.32	1.47	0.015
Fe	1.83	0.82	16.7	0.17
Ti	0.20	0.09	1.28	0.013
Ba	0.28	0.13	2.49	0.025
Ca	17.58	7.89	30.08	0.30

	Raw Coal ash	Raw Coal[a]	Acid Washed coal ash	Acid Washed[b] coal
V	0.018	0.008	0.075	0.0008
Cr	0.0009	0.0004	0.067	0.0007
Mn	0.036	0.016	0.13	0.0013
Co	0.0071	0.0032	0.012	0.0001
Ni	0.0015	0.0007	0.041	0.0004
Cu	0.0046	0.0021	0.122	0.0012
Zn	0.011	0.0048	0.026	0.0003
Sr	0.058	0.026	0.060	0.0006
Cd	0.00004	0.00002	0.020	0.0002
Pd	0.018	0.0078	0.161	0.0016

a. 44.9% ash
b. 1 % ash

Table X. Quantities of metal ions which may be extracted from Fruitland Formation coal by water .

Analyte	ng analyte/g coal
Na	787.8
K	8.01
Li	0.68
Mg	0.58
Ni	0.0
Cr	0.0
Co	0.0
Cu	0.0
Mn	0.0
Cd	0.06
Pb	0.0
Zn	0.0
Fe	0.0

too close to the chamber in one location so holes were burned through the glass walls of the sample chamber. The manufacturer has supplied us with an improved coil which has been installed. Ashing experiments are now in progress.

7. Rock Baseline Studies

Sections of the core sample from well GT-1 were taken above and below the coal seam. X-ray diffraction, thin-section petrographic, and air permeability and porosity tests were made on these segments. The detailed sample locations are GT-1 493.5' and GT-1 519.5' for the overburden and underburden, respectively. The results are reported in Table XI. In both instances it is evident that the rock is composed almost entirely of quartz, feldspar and clay. In both samples clays make up almost 30% of the rock. This number varies quite dramatically with location and we have found many sections of the core with clay-size particles making up more than 60% of the sample. The principal clay minerals are kaolinite and montmorillonite. The large quantity of clay in the overburden is particularly significant for the self-cleaning of groundwater that becomes contaminated as a result of UCG since clays are good, natural ion exchangers. For finely ground samples of overburden and underburden, cation exchange capacities of 2.7 meq/100 g rock and 2.2 meq/100 g rock, respectively, were determined by the nickel(I) ammine complex method (14). These values are reasonable for rock containing approximately 30% clay, but it is difficult to be quantitative because of the well-documented variability of cation exchange capacity with method (15). It is possible to conclude however that there is potentially a very large sink in the clays of the overburden for cations that complex with clays more strongly than the naturally dominant ions Na^{+} and Al^{+3}. The sorption studies are the focus of the leaching experiments described below.

The thin-section petrographic analysis of segments of overburden, stringer, and underburden were provided by Mr. R. Hicks of the Geology Department of the

Table XI. Physical and thermal properties of the over- and underburden from the GT-1 core.

Property Sample #	Overburden 28	Underburden 80	
Permeability (md)	0.017	0.014	
Porosity (percent)	8.1	7.7	
Minerals	Whole Rock	Clay (28%)	Whole Rock
Quartz (percent)	47		45
Feldspar	25		26
Kaolinite/Chloride	17	49	14
Illite/Mica		5	2
Montmorillonite	11	45	13

Property Sample #	Overburden 30	 31	Underburden 78	 79	 80
Tensile Strength (lb/in^2)					
Axial	92	50	100	28	43
Radial	149	85	100	135	135
Compressive Strength (lb/in^2)					
Axial	3259	2963	4108	783	812
Radial	3311	2849	4200	864	799
Thermal Conductivity @ 100°C cm sec°C Cal	0.0057	0.0063	0.0060	0.0047	0.0058
Heat Capacity @ 100°C gm°C Cal	0.217	0.236	0.219	0.187	0.188
True Density (gm/cc)	2.255	2.262	2.257	2.263	2.619

University of New Mexico. The results for each of these sections will be discussed in turn.

The Kirtland shale overburden is a rather simple geologic formation. It is an organic-rich claystone which is quite homogeneous. The organic material appears with no preferred orientation in a matrix of clay-size particles. It is a clay-supported matrix. These are small pieces of angular quartz found throughout the matrix. Just how much of the fine particles are actually clay minerals or what kind of clay mineral cannot be determined on the basis of this examination. Using this information however we plan to further characterize the clay minerals through an X-ray diffraction study.

The stringer that appears at about 500 ft. has a much more complex structure. It is a mixture of claystone and siltstone in which there is an abundant amount of organic material. There is also a good deal of authigenic material present. In one thin-section the sediment was an organic-rich claystone with authigenic clay, probably illite, present in fairly large quantities. In another particularly interesting thin-section the principal material was opaque carbonaceous matter present in very thin laminae alternated with angular clastic grains of quartz and plagioclase. The laminae are so thin as to suggest that their structure resulted from daily changes. Once again the authigenic clay mineral illite is found, this time in the lamella. There is also another mineral present in fairly large quantitites. In some thin-sections it has a vermiform appearance, while in other thin sections it seems to be more clearly crystalline. The identity cannot be established without X-ray diffraction work but it is probably gypsum or anhydrite since it appears to be authigenic, though some grains may be detrital. Calcite is also quite common in these thin sections. In addition, pyrite crystals are easily observed in the cubic and anhedral forms. We plan to study the environment of these crystals more carefully with a scanning electron microscope. We will also have photographs from these thin-sections to submit in the near future.

Pictured Cliffs sandstone is the generalized term given to the underburden. From the thin-sections taken from this area it is further identified as a claystone-siltstone with no bedding recognizable even at a magnification of 400X. In some instances it is an organic rich material in which the organic components have no preferred orientation. The biological source material cannot be clearly established though some pieces are probably cross sections of twigs which have been coalified and which have begun to migrate into the surrounding material. This appears to consist of very angular detrital clasts with a cherty cement. Some authigenic clays, most likely illite, were observed. Anhedral crystals of pyrite were found in this region as well.

Samples of both Kirtland shale (overburden) and Pictured Cliffs sandstone (underburden) were fused with lithium metaborate, dissolved and analyzed for metal ion concentrations by AA.

The fusion data are collected in Tables XII and XIII. In Table XI the major components of the over- and underburden and the associated clays are presented as percent of the oxides. The trace metal compositions of the two rock sections and their clays are given in Table XII. Also included are data from a narrow stringer of mineral matter found in the coal seam. The composition of both sediments with respect to the trace metals investigated are very similar. There are a few significant differences, however; Kirtland shale appears to be considerably richer in both calcium and iron than Pictured Cliffs sandstone. This probably indicates the presence of gypsum or anhydrite and pyrite in the sections of Kirtland shale analyzed. Pyrites can be observed visually in Pictured Cliffs sandstone, so the iron found here is probably also associated with the pyrites.

Table XII. Major components in mineral samples (%).

	Overburden	Overburden clay	Stringer	Stringer clay	Underburden	Underburden clay
SiO_2	57.09	55.59	55.65	56.18	63.31	66.57
Al_2O_2	19.60	21.82	23.40	25.29	16.44	25.75
Fe_2O_3	3.06		1.18		2.09	
FeO	1.82		0.69		1.03	
MgO	1.19	1.48	0.95	0.98	0.66	1.07
CaO	0.27	0.27	0.29	0.13	0.09	0.05
Na_2O	1.46	2.07	1.70	2.41	1.46	0.96
K_2O	2.10	0.97	1.01	0.94	2.49	1.94
H_2O^+	7.91		8.53		8.49	
H_2O^-	4.22		5.51		1.53	
TiO_2	0.57	0.48	0.43	0.17	0.66	0.45
P_2O_5	0.029		0.032		0.027	
MnO	0.009	0.011	0.003	< 0.006	0.006	0.008
SrO	0.021	0.021	0.025	0.024	0.016	0.017
S	< 0.01		0.01		1.21	
Total (as Fe_2O_3)	5.08	5.47	1.95	1.62	3.22	2.15
L.O.I. (1000°C)	7.73		8.53		8.38	

Table XIII. Trace composition of mineral samples (%).

	Overburden	Overburden clay	Stringer	Stringer clay	Underburden	Underburden clay
Cr	0.0019	0.0025	0.00126	0.00127	0.00191	0.00352
Co	0.0053	0.0053	0.00353	0.00480	0.00557	0.00491
Ni	0.00323	0.00143	0.000	0.00030	0.00104	0.00300
Cu	0.00562	0.00304	0.00248	0.00151	0.00469	0.00350
Zn	0.00655	0.00867	0.00346	0.00147	0.0128	0.00710
Cd	0.00243	0.00039	0.00032	0.00011	0.00026	0.00004
Ba	0.0151	0.000	0.0300	0.0301	0.0228	0.00760
Pb	0.0122	0.0121	0.0105	0.00518	0.0140	0.0128
V	0.0236	0.0121	0.000	0.0059	0.0117	0.0100

The major elemental components in the Kirtland shale overburden, the clay-sized minerals of the overburden, the stringer and its clay, and the coal ash are all compared in Table XIV. The most outstanding variation that can be seen is the difference in iron composition. The overburden is relatively rich in iron and the iron is associated with the clay-sized particles of the overburden. Other differences are so small that they may not be significant.

8. Leaching and Ion Exchange Studies

This area of study deals with the determination of adsorption coefficients, K_d's, and ion-exchange constants, k_d's. The subject area is quite complex and is one that has been approached by others from a number of points of view. It is complicated by the fact that we are dealing with a heterogeneous natural system in which both adsorption and ion exchange may occur simultaneously and by the large quantity of clay, a natural ion exchanger. One of the first concerns has been separating adsorption from ion exchange and another has been identifying the contribution to both adsorption and ion exchange that is made by rock, coal, and clay independently. This section describes our initial experiments aimed at clarification of these questions and presents the results which have been obtained. All the experiments reported here were performed by the static, or batch, method. In this method a solution containing the test ion(s) is equilibrated with the solid, the solid is then removed by filtration or centrifugation and the solution is analyzed by AA for the metal ions of interest. Columns have been constructed for dynamic leaching studies and preliminary experiments are underway, but no data is reported at this time.

Table XIV. Comparison of major components in coal and overburden and stringer (%).

	Overburden	Overburden clay	Stringer	Stringer clay	Raw Coal ash	Raw Coal*
Si	26.67	25.99	26.02	26.67	19.58	8.79
Al	10.37	11.55	12.39	13.39	11.56	5.19
Na	1.08	1.52	1.26	1.78	1.75	0.79
K	1.74	1.65	0.84	0.78	0.77	0.35
Mg	0.71	1.90	0.59	0.60	0.72	0.32
Fe	3.56	3.83	1.36	1.13	1.83	0.82
Ti	0.34	0.29	0.26	0.10	0.20	0.09
Ba	0.015	0.00	0.03	0.03	0.28	0.13
Ca	0.19	0.19	0.21	0.065	17.58	7.89

*44.9% ash

A number of experiments have been performed. In one experiment 5 g samples of underburden (Pictured Cliffs sandstone) were equilibrated with solutions of HNO_3 or NaOH covering the pH range of 1-12. The resulting solutions were examined for the anions Cl^-, F^-, CN^-, and $SO_4^=$ and for total dissolved solids. The results are given in Table XV. Concentrations of Cl^-, F^-, and CN^- were determined using ion selective electrodes and $SO_4^=$ was determined by a standard spectrophotometric method.

Several interesting conclusions can be drawn from these results. First of all, it is clear that the rock has a strong buffer action which holds the pH of the solutions at about 7.2 This effect may be due to the hydroxyl groups on the clay minerals. The final pH of 7.2 is considerably lower than the pH of the water samples removed from the two wells; the reason for this higher acidity is not clear. Second, a plot of TDS vs. initial pH, Figure 12, shows that a large quantity of rock is dissolved in either strongly acidic or strongly basic solutions with a minimum TDS in the vicinity of pH 7. Third, by far the greatest quantity of anion, is sulfate. The concentrations of chloride, fluoride and cyanide were so low at all pH values that the variations are insignificant. In a general way, the quantity of sulfate parallels TDS though the variations are not as dramatic. It is also clear that at the extremes of the pH range examined $SO_4^=$ makes up only a small fraction of the total dissolved solids whereas at pH 7, almost all of the total dissolved solids are sulfate salts, presumably Na_2SO_4, K_2SO_4 and $CaSO_4$.

Table XV. Total dissolved solids and concentrations of Cl^-, F^-, CN^- and $SO_4^=$ extracted from Pictured Cliffs sandstone as a function of pH.

Initial pH	Final pH	TDS, mg/ℓ	$[Cl^-]$, mg/ℓ	$[F^-]$, mg/ℓ	$[CN^-]$, mg/ℓ	$[SO_4^-]$, mg/ℓ
1.05	--	15610	0.753	0.37	0.021	653
2.08	7.14	2620	0.623	0.12	0.028	436
3.03	7.26	1570	0.653	0.18	0.028	462
4.04	--	860	0.643	0.21	0.027	443
5.02	7.22	830	0.643	0.19	0.024	424
6.01	7.24	--	0.623	0.20	0.013	481
7.01	7.12	690	0.623	0.20	--	424
8.01	7.24	--	0.663	0.20	0.012	443
9.02	7.18	740	0.633	0.20	--	436
10.02	7.18	--	0.653	0.20	0.011	399
11.00	7.26	930	0.653	0.21	--	558
12.05	--	1660	0.653	0.39	0.010	434

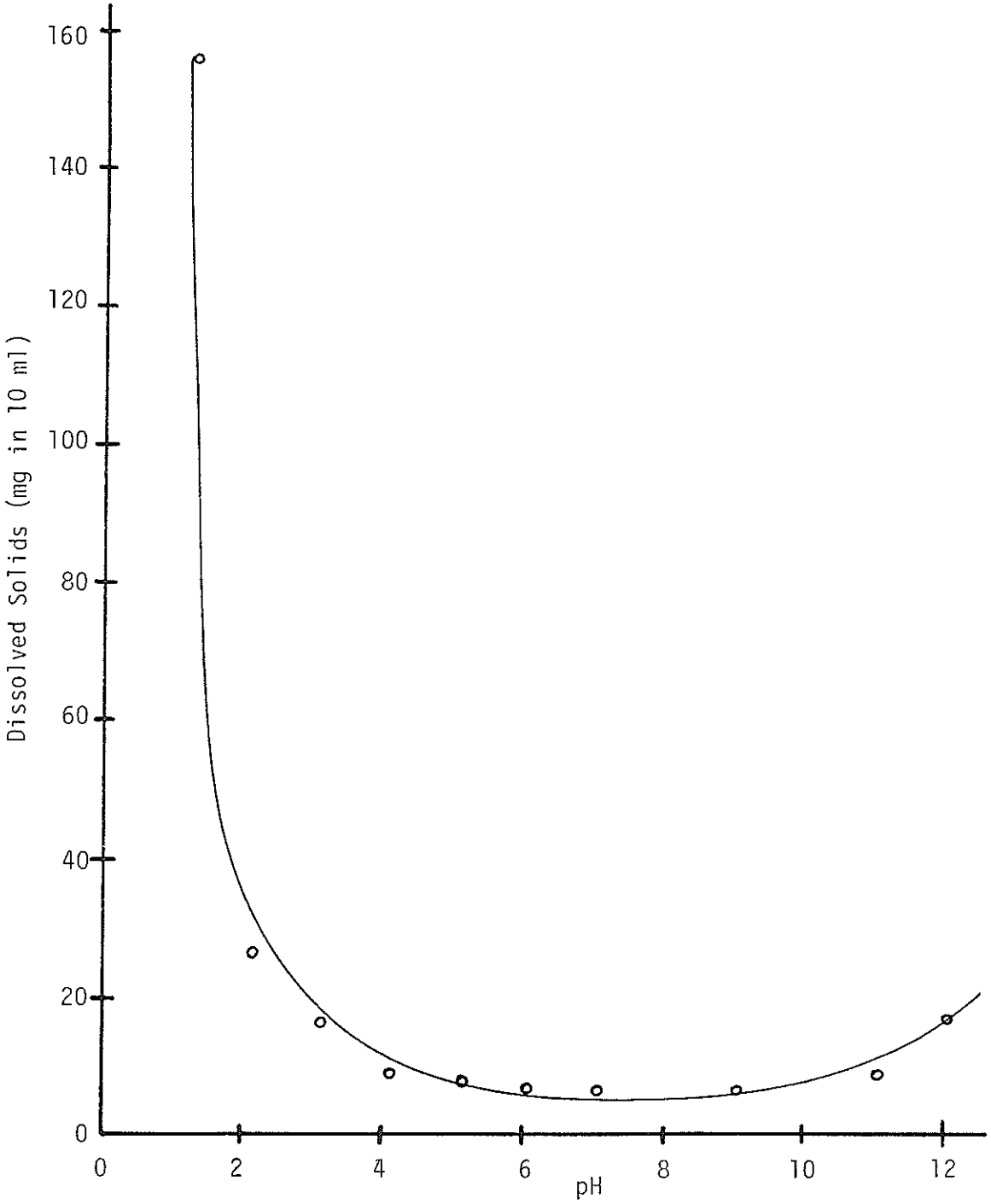

Figure 12. Total dissolved solids from Pictured Cliffs sandstone as a function of initial pH.

A related experiment was performed with the Kirtland shale overburden. A sample of Kirtland shale was shaken with sufficient HNO_3 or NaOH to adjust the pH of the solution to a preselected final value. If the desired pH was not obtained with a single addition more acid or base was added gradually and the mixture was agitated until the final pH was reached. This procedure generally required several days. The mixture was filtered to remove rock and clay and then the filtrate was analyzed for metal ion concentrations by AA. The metals studied over the pH range of 1 to 10 were manganese, sodium, barium, calcium, chromium, iron, magnesium, zinc, copper, cobalt, nickel, aluminum, lead, cadmium, lithium, and silver. For a number of the metals (Mn, Ba, Cr, Cu, Co, Ni, Pc, Bd, Ag) the amounts in solution at final pH values higher than about 5 were so low that they could not be determined reliably, so the effect of pH is known only over the range of 1 to about 5. In each case however there is a decrease in the amount of metal in solution from a high value near pH 1 to a much lower value as the pH increases. Manganese is a representative example; its behavior is shown in Figure 13. For metals for which the concentration could be determined over the entire pH range there is the same general decrease in metal ion concentration to a minimum in the vicinity of pH 6-7; in some cases (Fe, Zn, and Al) the concentration increases as the pH approaches pH 10. The most dramatic of this behavior is exhibited by aluminum, as shown in Figure 14. More common is the performance of magnesium, Figure 15, which decreases in concentration to ever lower values or minimum values as pH increases. This experiment accounts for the very low concentrations of a number of metal ions in groundwater taken from wells GT-1 and GT-2 even though fusion tests showed these metals are present in appreciable quantities in Kirtland shale, coal, and Pictured Cliffs sandstone.

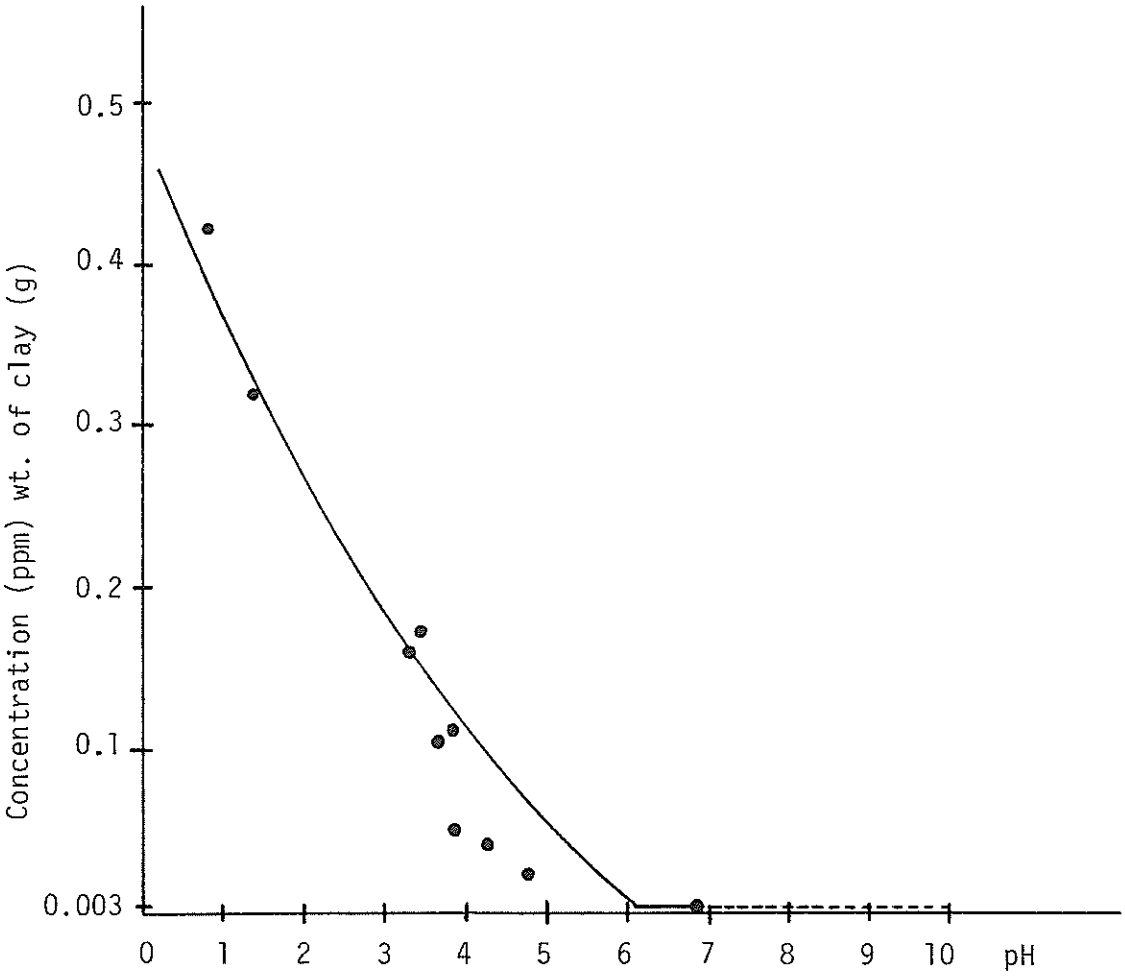

Figure 13. The amount of manganese dissolved from Kirtland Shale as a function of final pH.

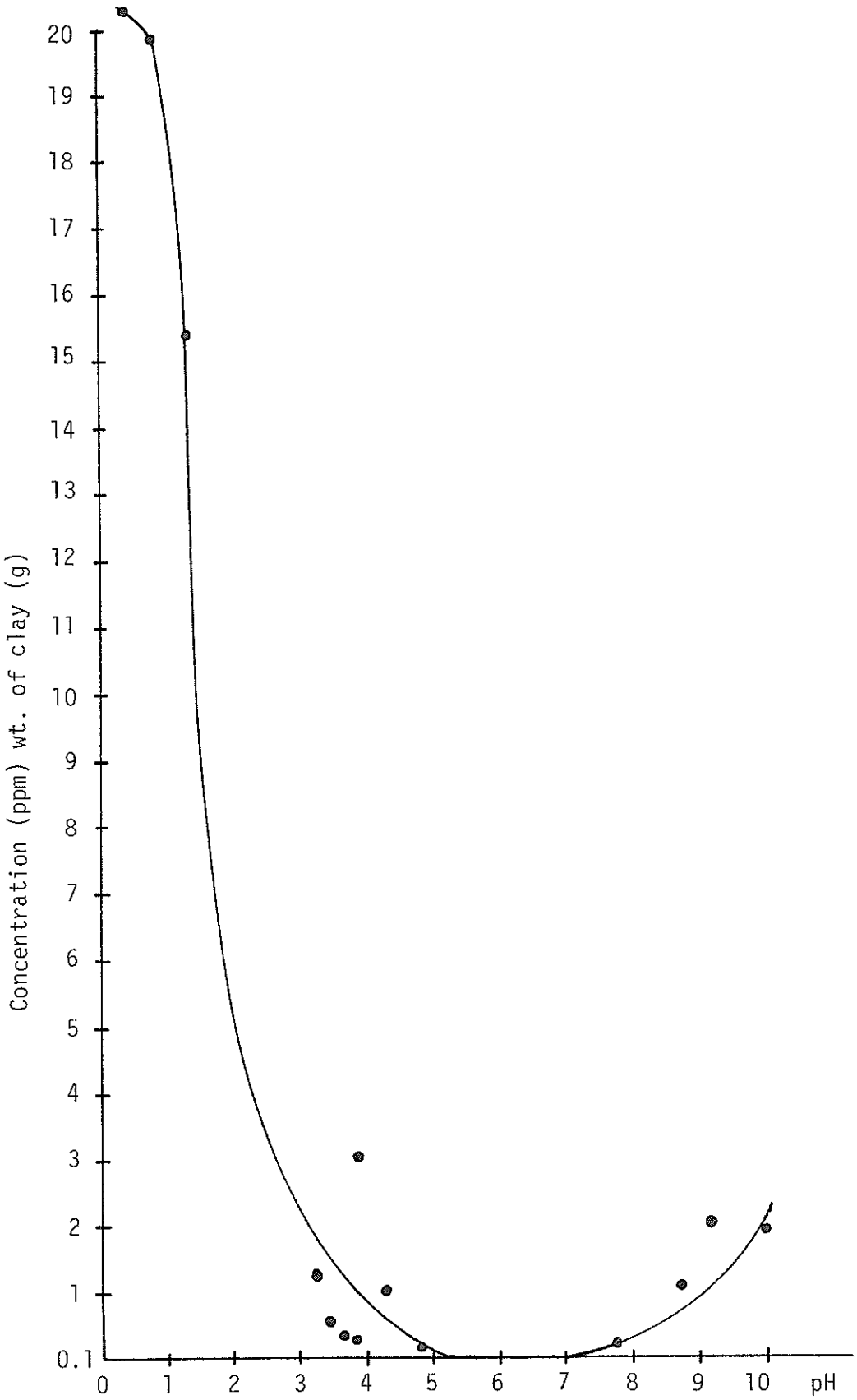

Figure 14. The amount of aluminum dissolved from Kirtland Shale as a function of final pH.

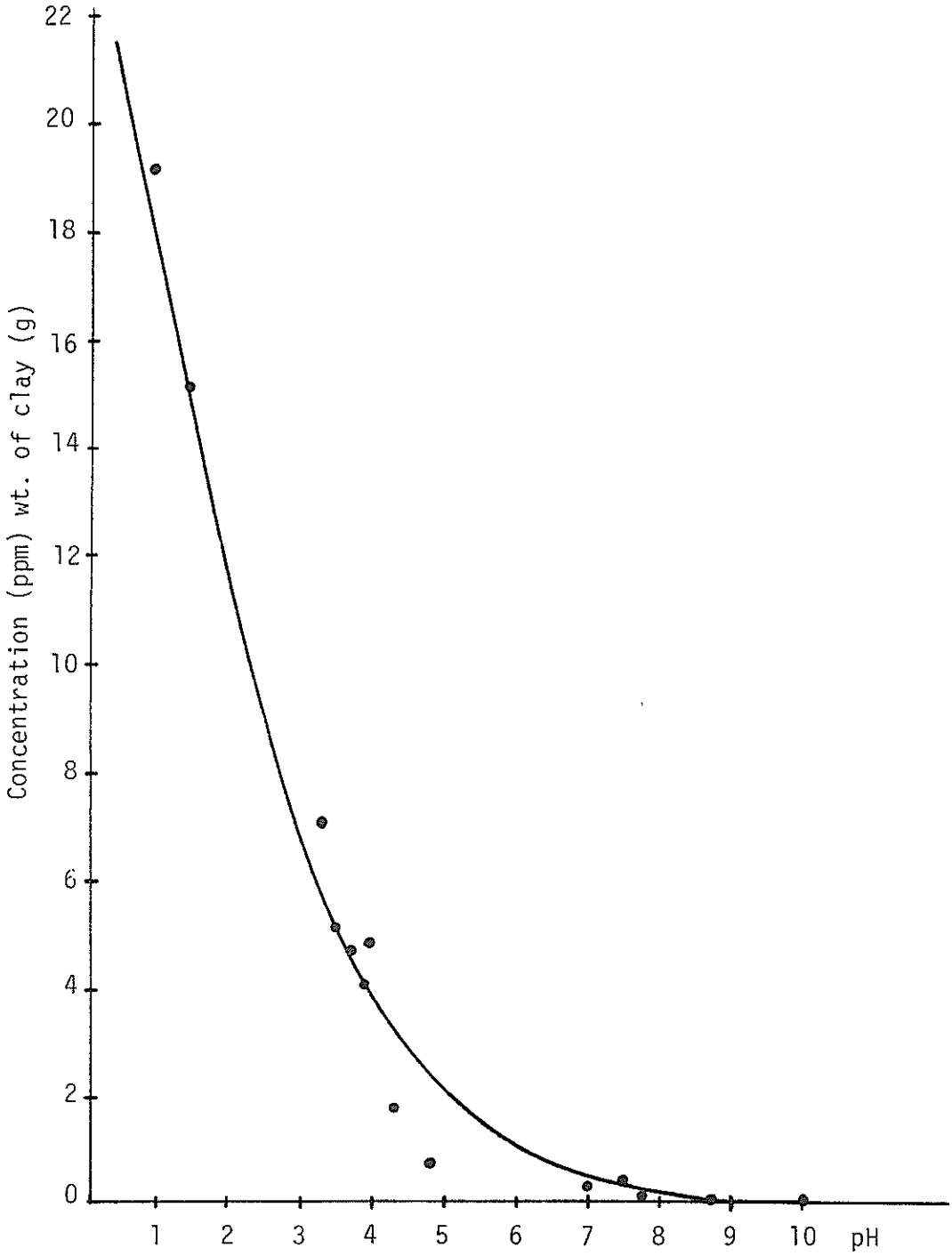

Figure 15. The amount of magnesium dissolved from Kirtland Shale as a function of final pH.

Some studies on the determination of adsorption coefficients, K_d's, and their dependence on such factors as concentration and particle size have been initiated. For example, aqueous solutions of $Cd(NO_3)_2$ were equilibrated with known quantities of overburden or underburden of a certain particle size range and the resulting solutions were analyzed for Cd^{+2} remaining in solution. K_d values were calculated from these data for all concentrations and particle sizes. The results of this experiment are reported in Table XVI. These results show a definite particle size effect which is most evident for the smallest particles The effect is that K_d is reduced when the particle size has reached -100 mesh (<0.0058" in diameter). The reduction in K_d is significant; it is about a factor of 4 less than K_d observed in the next largest, 7-12 mesh (0.055-0.110" diameter), particle size range. In each instance K_d increases with increasing concentration to a maximum in the vicinity of 100 mg/ℓ and then decreases rather abruptly. This is shown graphically in Figures 16 and 17.

At the time the solutions were analyzed for loss of cadmium they were also monitored for the appearance of Mg^{+2}, Na^+, K^+, and Ca^{+2}. The results for Ca^{+2} are not available yet, but the amounts of desorbed Mg^{+2}, Na^+, and K^+ are shown in Table XVII. The effect of particle size can be seen once again at the smallest size used in this experiment (0.058" or 150 μm). The more interesting result is the observation that for each concentration range the amount of desorbed cation remains low until the concentration of added Cd^{+2} reaches 1000 mg/ℓ at which point there is an abrupt increase, by a factor of three or more, in the amount of desorbed metal ion. Although this effect has not been explored thoroughly, our preliminary hypothesis is that at low $[Cd^2]$ values cadmium is being adsorbed at the surface, displacing a few metal ions that we observed. When $[Cd^{+2}]$ increases to the range of 100-1000 mg/ℓ ion-exchange becomes important and much larger quantities of metal ions are displaced from exchange sites.

Table XVI. K_d values for Cd^{+2} on overburden and underburden of different particle sizes.

Sample	Particle size	$[Cd^{+2}]$ mg/ℓ	initial pH	final pH	K_d*
Overburden	passed 4 mesh	0.04	10.36	10.20	131
		0.85	10.32	10.18	279
		11.1	10.29	10.24	1279
		111	9.75	9.67	1775
		1110	6.98	6.94	61.3
	7-12 mesh	0.04	10.36	10.27	134
		0.85	10.32	10.20	460
		11.1	10.31	10.17	1043
		111	9.79	9.43	1294
		110	7.10	6.89	71.6
	-100 mesh	0.04	10.32	10.04	67.6
		0.85	10.31	10.13	131
		11.1	10.27	10.11	246
		111	9.65	9.33	374
		1110	6.96	6.68	28.4
Underburden	passed 4 mesh	0.04	8.40	8.22	(130)
		0.85	8.02	7.10	923
		11.1	6.83	6.59	989
		111	6.70	6.12	1209
		1110	6.28	5.78	96.2
	7-12 mesh	0.04	10.51	9.80	(140)
		0.85	10.48	10.14	554
		11.1	10.45	10.27	755
		111	9.90	9.76	1145
		1110	10.30	9.91	108
	-100 mesh	0.04	10.43	9.90	73
		0.85	10.44	10.17	132
		11.1	10.40	10.13	168
		111	9.81	9.54	302
		1110	7.30	7.01	44.7

*$K_d = \frac{\text{g adsorbed x volume}}{\text{g in soln x wt. sample}}$

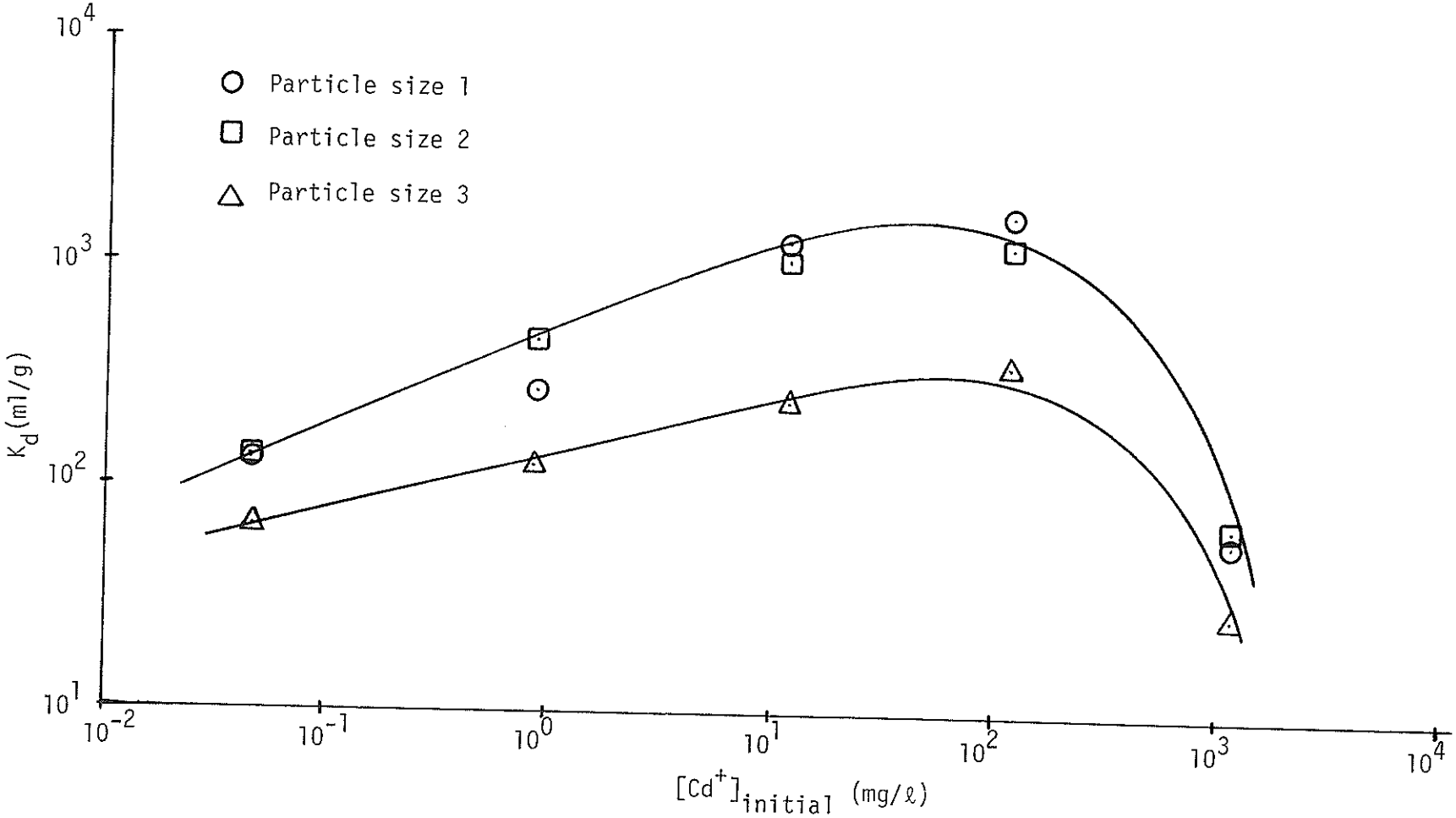

Figure 16. K_d for Cd^{+2} or Kirtland shale as a function of initial concentration of Cd^{+2}.

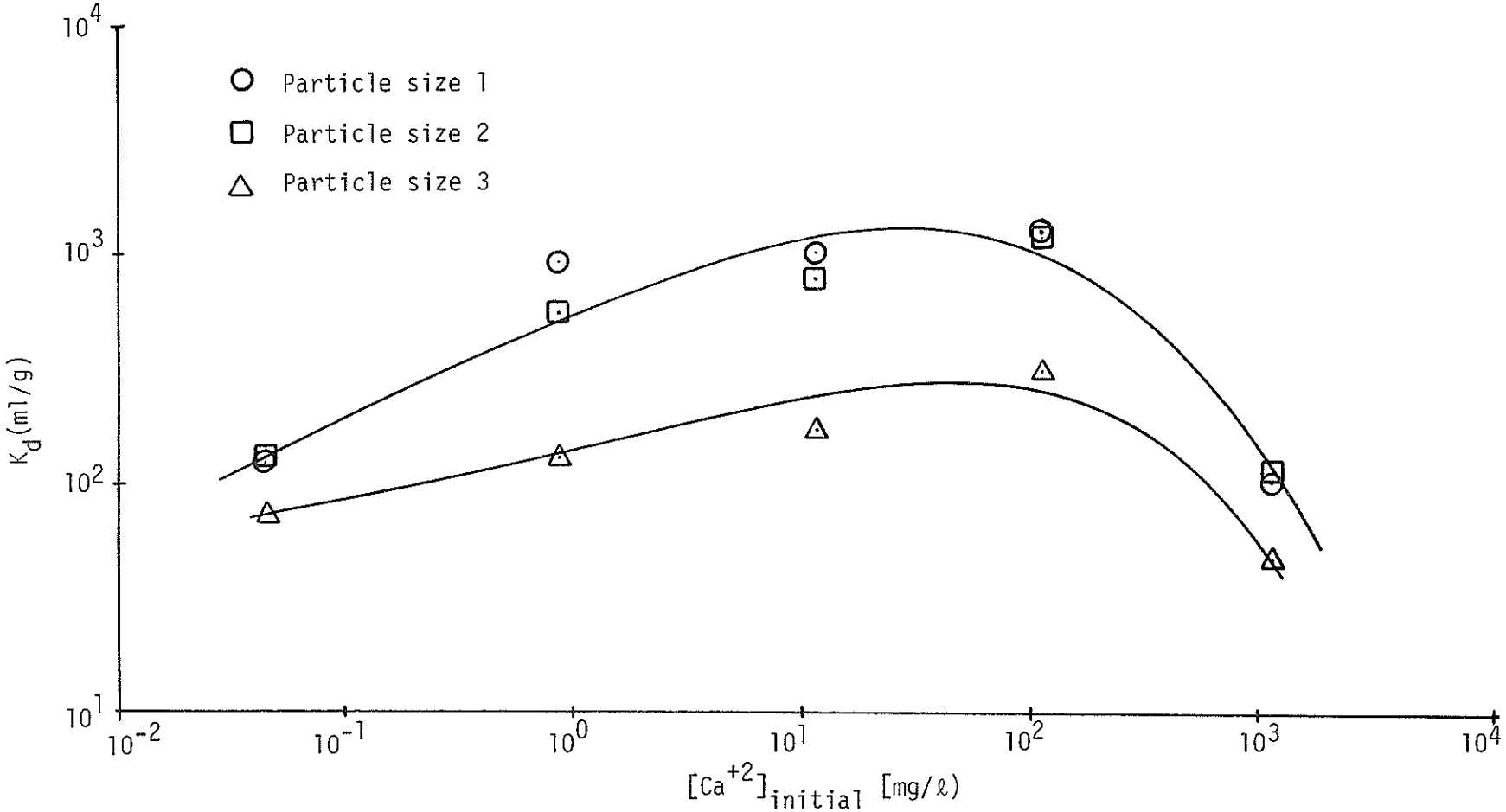

Figure 17. K_d for Cd^{+2} on Pictured Cliffs sandstone as a function of initial concentration of Cd^{+2}.

Table XVII. Quantities of Mg^{+2}, Na^{+} and K^{+} desorbed from overburden and underburden by Cd^{+2}.

Sample	Particle size	$[Cd^{+2}]_{initial}$ mg/ℓ	$[Mg^{+2}]$ mg/ℓ	$[Na^{+}]$ mg/ℓ	$[K^{+}]$ mg/ℓ
Overburden	passed 4 mesh	0.04	0.071	25.8	5.52
		0.85	0.165	24.1	4.69
		11.1	0.153	26.1	4.47
		111	0.144	18.8	4.19
		1110	1.151	121.5	12.76
	7-12 mesh	0.04	0.174	30.7	5.21
		0.85	0.178	28.4	5.23
		11.1	0.174	25.4	5.27
		111	0.167	21.3	5.01
		1110	0.052	118	12.5
	-100 mesh	0.04	0.300	31.1	9.83
		0.85	0.332	26.4	10.61
		11.1	0.330	27.4	10.83
		111	0.297	21.3	10.68
		1110	2.6	74.4	14.4
Underburden	passed 4 mesh	0.04	0.168	22.5	5.16
		0.85	0.150	16.0	4.37
		11.1	0.160	14.5	4.49
		111	0.140	15.8	4.65
		1110	0.367	127	11.6
	7-12 mesh	0.04	0.168	20.9	4.94
		0.85	0.164	14.4	4.46
		11.1	0.175	10.8	5.57
		111	0.144	15.6	4.70
		1110	0.348	115	11.6
	-100 mesh	0.05	0.268	24.4	9.76
		0.85	0.278	18.9	10.5
		11.1	0.303	21.7	12.1
		111	0.264	35.2	10.6
		1110	0.806	93.8	14.4

It is useful to plot the cadmium adsorption data in two other ways. In the first variation we plot the quantity of cadmium adsorbed per gram of rock (mg Cd^{+2} adsorbed/g rock) as a function of the quantity of cadmium left per milliliter of solution (mg Cd^{+2} in soln/ml soln). The graph is shown in Figure 18. The interesting feature of this graph is the gradual approach to saturation of the rock by Cd^{+2} as the concentration of Cd^{+2} in solution increases. This limit should be the cation exchange capacity of the rock with respect to cadmium. Extrapolation of the graph to the asymptotic limit gives a cadmium ion exchange capacity of 8-10 meq/100 g rock. This value is in reasonable agreement with that obtained by a more conventional approach.

An alternative treatment of the data is the isotherm approach. In Figure 19 the quantity of Cd^{+2} adsorbed per gram of rock is plotted as a function of the initial concentration of Cd^{+2}. This plot is linear on a log-log scale. Behavior of this sort is known as a Freundlich isotherm; it is commonly observed for adsorption of solutes on a solid phase. This is an empirical relationship, so the slope and intercept cannot be ascribed any particular physical significance, though this behavior is generally regarded as indicative of a heterogeneous surface. The slope and intercept are frequently associated with the adsorption capacity and adsorption strength of the system; these values will be reported for several ions later. It is interesting that the results for both Kirtland shale and Pictured Cliffs sandstone lie on the same line; this may merely indicate that the Freundlich isotherm is not a very sensitive way to display adsorption data.

The adsorption coefficient, K_d, of Mg^{+2} on Kirtland shale was also determined. In this experiment K_d was determined for a solution of magnesium ion at a fixed concentration over Kirtland shale not sorted according to size but as a function of final pH of the solution over the pH range of 2.83 to 4.16. The pH was adjusted with nitric acid. A plot of K_d (Mg^{+2}) vs. pH is shown in Figure 20.

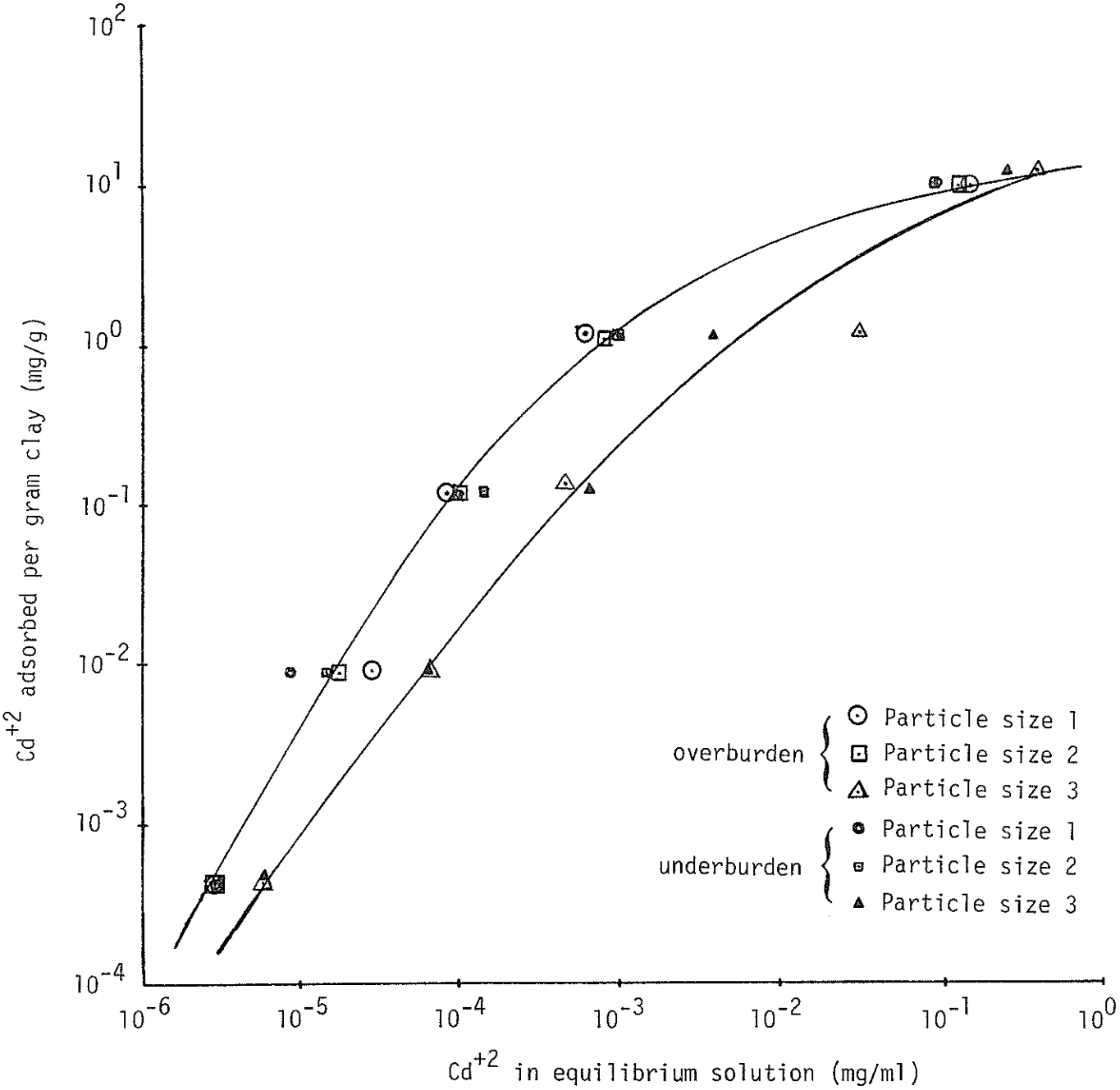

Figure 18. The amount of Cd^{+2} adsorbed per gram of rock as a function of the concentration of Cd^{+2} remaining in solution.

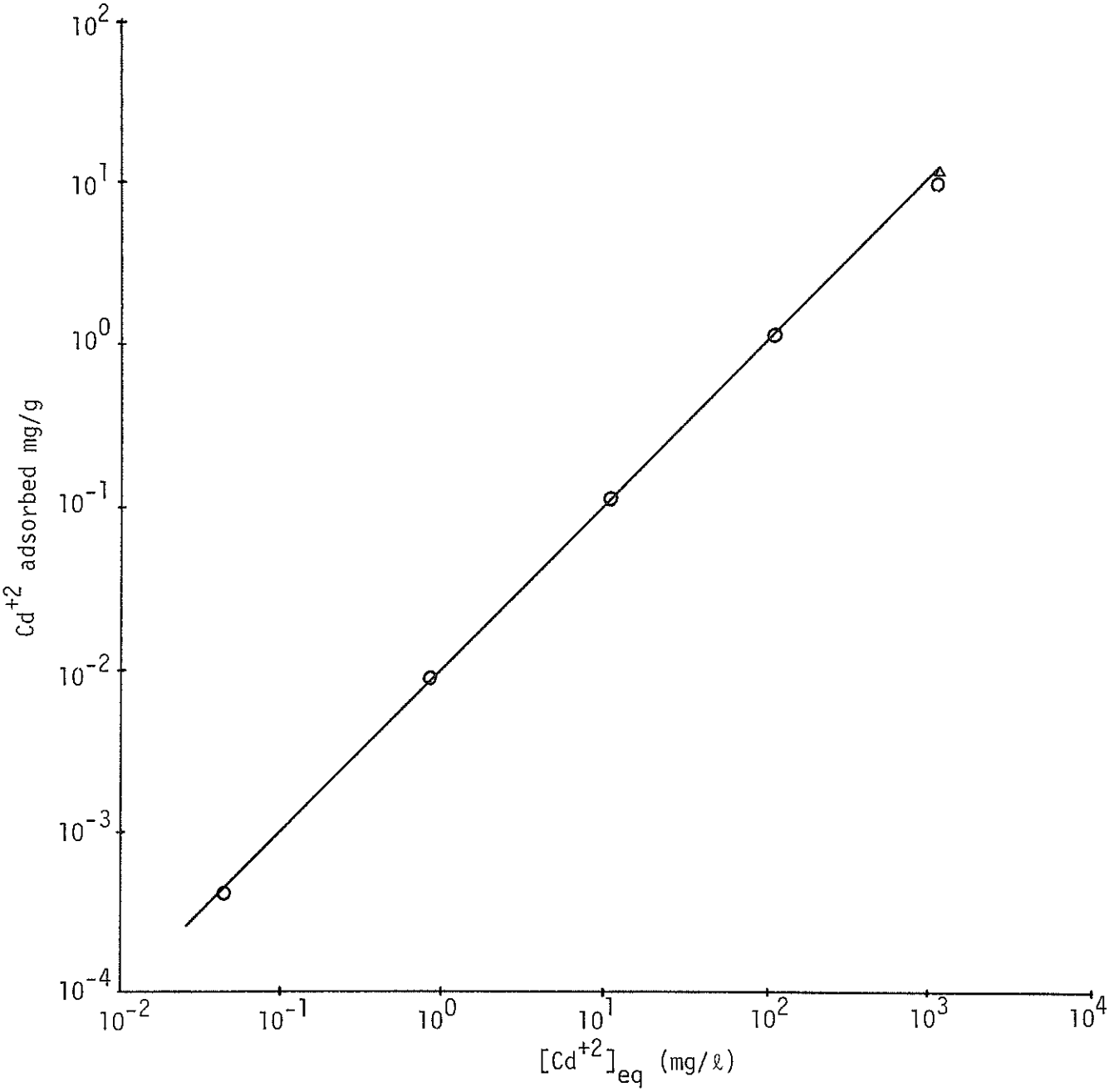

Figure 19. The amount of Cd^{+2} adsorbed per gram of rock as a function of initial concentration (all particle sizes, for both underburden and overburden, fell very close together. Thus each circle represents 6 points except: the triangle represents the one exception where particle size 3 gave a point apart from the others).

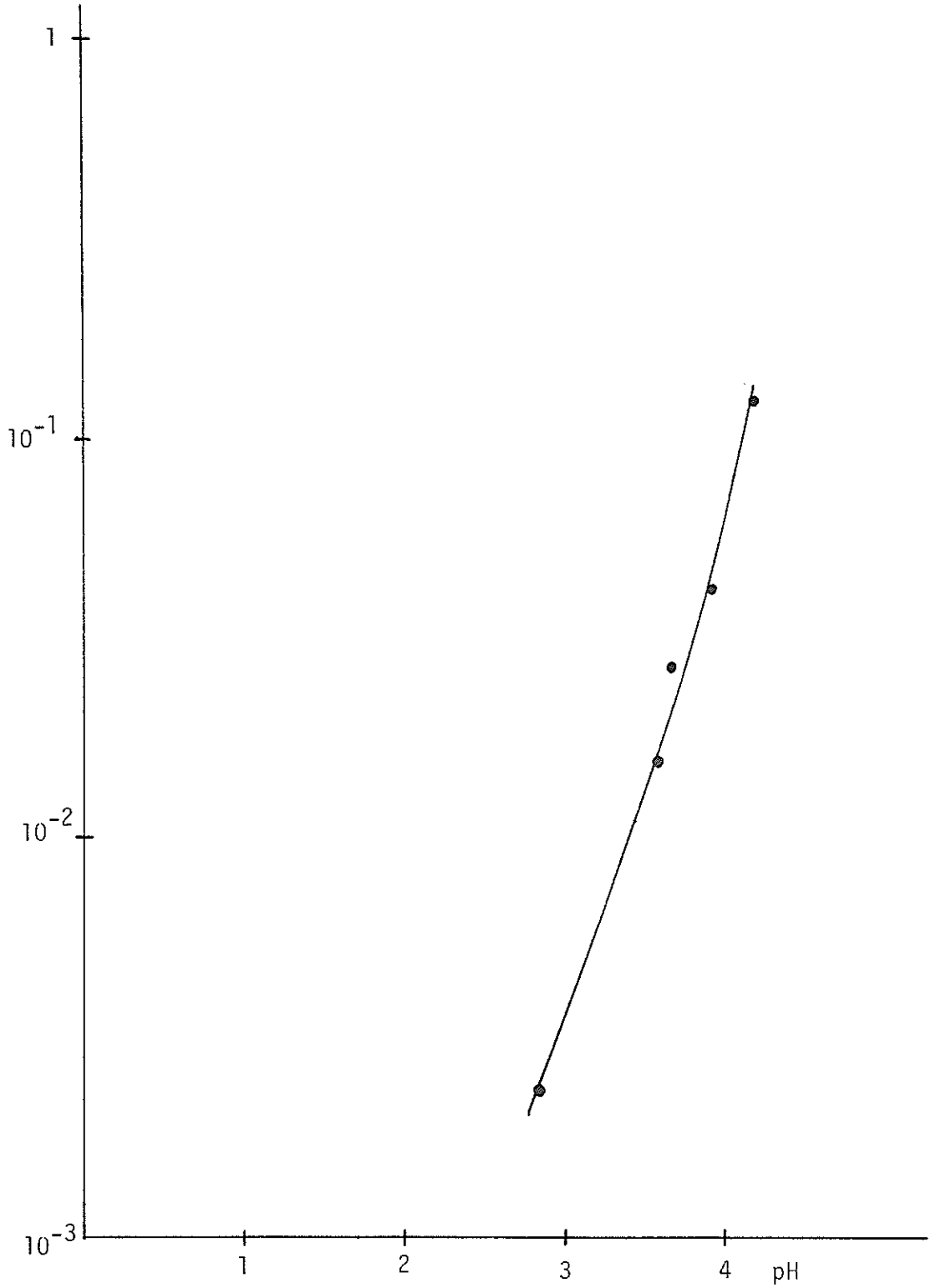

Figure 20. K_d for Mg^{+2} on Kirtland Shale as a function of pH.

Under this set of conditions K_d increases rather sharply with increasing pH. Since the final pH ranges studied for the K_d values of Mg^{+2} and Cd^{+2} were not the same it is difficult to compare K_d values directly. Extrapolation is also rather tenuous, but suggests that at the same pH the two metal ions will have similar K_d's.

Some sorption studies have been initiated with coal. In these studies sorption on coal was studied as a function of particle size, pH and temperature. Raw coal was equilibrated with solutions of various metal ions (Ca, Fe, Al, Na, Mn, Zn, H) for several days, centrifuged or filtered, and the filtrate was analyzed for metal ion concentration by AA. In one set of experiments an attempt was made to determine how much of the observed effects are due to the minerals in coal so a sample of Fruitland Formation coal was subjected to an HCl-HF acid wash (16) to remove all the minerals. This coal was then treated with metal ion solutions as described above.

The K_d values obtained in these experiments are reported in Table XVIII. When these data are plotted as isotherms, quantity of ion adsorbed per gram of rock vs. initial ion concentration, the results are found to fit the Freundlich isotherm equation, usually with a very high correlation coefficient, $r > 0.98$. The slope and intercept data are currently being evaluated for adsorption strength and capacity numbers. Data for adsorption of Al^{+3} and Na^{+} are not given in Table XVIII because aluminum was so strongly adsorbed that in all cases $K_d(Al^{+3}) = \infty$ and because sodium gave anamolous and irreproducible results whose interpretation is not satisfactory at this point. The data in Table XVIII for raw coal show that all the ions studied are adsorbed to varying degrees and that K_d decreases as the initial ion concentration increases. This is consistent with the interpretation that there are a limited number of adsorption sites on the

Table XVIII. K_d's for metal ions on raw and treated Fruitland Formation subbituminous coal.

Sample	$[Ca^{+2}]^*$ mg/ℓ	K_d	$[Fe^{+3}]$ mg/ℓ	K_d	$[Mn^{+2}]$ mg/ℓ	K_d	$[Zn^{+2}]$ mg/ℓ	K_d
Raw Coal	115.4	1.30	40.5	∞	4.33	21.8	3.94	∞
	156.6	0.253	113.3	514	8.81	5.25	9.92	40.4
	266.0	-0.336	233.7	274	12.70	3.29	20.09	33.7
	560.0	-0.677	427.5	22.9	21.80	1.04	34.93	10.3
Treated Coal	55.4	-0.25	19.9	-0.154	1.49	-0.140	1.22	-0.121
	111.7	0.064	39.4	-0.224	3.64	-0.123	2.89	-0.117
	221.7	0.041	78.6	-0.346	7.49	-0.151	5.94	-0.155
	502.7	-0.151	138.1	-0.290	14.9	-0.148	11.31	-0.120

*The concentrations are reported as initial concentration of the ion before adsorption occurs.

coal-mineral combination that we term "raw coal" and that as the initial metal ion concentration increases there are fewer and fewer sites available to accept the addional ions.

The experiment with treated coal is quite enlightening. The acid washing process is intended to remove all mineral matter from the coal. The fact that negative K_d values are obtained for nearly all cases indicates two things: a) there still are metal ions associated with the coal, whether they are in minerals in coal or chelated to coal is not clear, and b) most of the adsorption sites in raw coal are in fact adsorption sites on coal-associated minerals. Experiments to clarify the situation are in progress. First of all, a lithium borate fusion will be performed on treated coal to establish the quantities of metal elements still present. Next, a set of high and low temperature ashing experiments will be performed to identify the minerals in raw coal so they may be examined independently.

The effect of particle size on K_d's of Fe^{+3}, Al^{+3}, Zn^{+2}, and Mn^{+2} for raw coal is summarized in Table XIX. For these metal ions K_d drops with decreasing particle size, generally reaching a plateau value by the time the mean particle size is 1 mm.

Table XIX. The effect of coal particle size on K_d of Fe^{+3}, Al^{+3}, Zn^{+2} and Mn^{+2}.

Particle size, mm	$[Fe^{+3}]$ mg/ℓ	K_d	$[Al^{+3}]$ mg/ℓ	K_d	$[Zn^{+2}]$ mg/	K_d	$[Mn^{+2}]$ mg/	K_d
4	120	210	51.1	∞	11.1	29.7	13.4	1.37
3		22.9		∞		10.3		1.02
2		1.50		9.63		1.75		0.164
1		1.31		9.63		1.58		0.101

Humic and fulvic acids are naturally occurring chelating agents that are commonly found in water that has percolated through decaying organic matter. It is likely that these or closely related acids will be found in groundwater of coal seams. It has been reported that humic acids dramatically reduce the K_d values for certain radioisotopes (17) so their mobility in the presence of humic acids is much greater than in water without humic acid. We are concerned with assessing the impact of this problem for UCG, so the sorption on coal experiments were also performed in the presence of some humic acid.

It was expected that the addition of humic materials to the simulated groundwater would result in lower K_d values because of soluble chelates formed between humic acid and the metal ions in solution. Instead we find just the opposite: increasing humic acid concentration is accompanied by an increase in the apparent K_d in the case of raw coal. No firm data are reported at this time because we are concerned that this may be an experimental artifact. In particular, the humic acid used was technical grade material, so it probably contained a large quantity ($\sim$20 wt%) of metal ions already chelated to it. We will analyze our humic acid by a lithium metaborate fusion and attempt to load the humic acid with a single cation, say H^+, by washing repeatedly with acid. In addition, K_d values in the presence of humic acid for treated coal are very similar to K_d's in the absence of humic acid. This suggests that the dominant process in the raw coal-humic acid experiment was an interplay between humic acid and coal-associated minerals. Interestingly, the data for metal ion adsorption in the presence of humic acid also fit a Freundlich isotherm with high precision. These results are being subjected to further and more detailed analysis.

We are also interested in trying to distinguish between adsorption and ion exchange. As discussed above, we may have observed the difference in these

two sorption mechanisms with the Cd^{+2} rock experiments. Two experiments specifically designed to sort out the two effects are planned; we have some very preliminary data from one experiment and we expect to begin the other soon. In the first case, a standard clay, calcium-montmorillonite, was added to a stirred solution containing Cu^{+2} ions at a concentration of 1000 mg/ℓ and the rate of disappearance of Cu^{+2} from solution was monitored by a copper ion selective electrode. The observed rate is independent of stirring rate so we are observing chemically controlled surface phenomena and not merely the physical process of transport to the surface. The observed rate has two clearly distinguished first-order components, one fast and the other considerably slower. We tentatively associate the faster one with adsorption and the slower one with ion exchange with the Ca^{+2} ions in the clay matrix. Temperature dependence studies are underway which should give heats of reaction for the two processes that will aid in further identifying the steps. Clay will be loaded with other metal ions prior to reaction with Cu^{+2} to learn more about the exchange reactions. Eventually we hope to apply the results from standard clays to rock from Kirtland shale and Pictured Cliffs sandstone.

In the other experiment, we plan to use a Tronac titration calorimeter to determine heats of reaction in a direct fashion for sorption of metal ions on clay, rock and coal substrates. Preliminary experiments are now in progress.

9. Organics in Water

Another important constituent of groundwater in the vicinity of a coal seam is the organic content. In the case of UCG, we are interested in how the baseline level of organics in water is modified -- that is, subtracted from or added to -- by the UCG process. During sampling of wells GT-1 and GT-2 several

samples were collected and preserved for later analysis of organics. Efforts along these lines are still in the early stages. They consist of getting into an operational configuration a CVC 2001 GC/MS in our laboratories. The time-of-flight mass spectrometer has been used for other experiments, but the gas chromatographic part has not been operated. We are building the appropriate columns and linking the two together through a jet separator. In the meantime the column materials are being tested separately on another gas chromatograph using calibrated mixtures of organics typical of those we expect to find in groundwater.

Phenols are expected to be one of the most significant organic groundwater contaminants resulting from a UCG burn. In order to be able to gain some insight into how serious a contamination problem phenols might be, we have undertaken a study of phenol adsorption by coal and minerals. The results of this study are included as Appendix C.

10. Analytical Methods

Most of the initial effort in the area of mastering or developing the analytical methodology necessary for the work proposed here was in the area of trace metal analysis using atomic absorption spectroscopy (AA). For many of the species of interest standard flame AA procedures can be used and these analyses have proceeded smoothly.

When more sensitivity is needed than can be provided by flame AA, a graphite furnace is used in place of the flame. For some species, especially the high boiling point species, the furnace is an excellent technique. For lower boiling point species, e.g. Pb and Cd, problems due to the high salt concentration of the water tested here have been manifested. Considerable effort has been put forth to understand the interference and in doing so eliminate the problems from the analysis.

A careful study has been made of the Cl^- interferences on the analysis of Pb in a graphite furnace. From the results obtained in our laboratory it can be concluded that the reaction

$$PbO(s) + C(s) \rightarrow Pb(g) + CO(g)$$

is responsible for the atomization on Pb. Thus, the availability of carbon is important and we obtained superior results using nonpyrolytic graphite rather than the standard pyrolytic graphite. Also, our results indicate that occlusion is the dominant physical interaction and the use of the nonpyrolytic graphite also helps reduce this problem. These results have been submitted to Analytical Chemistry and a copy is included as Appendix A.

Another area where effort has been expended is the use of ion selective electrodes. These are very useful because analyses can be performed in the field where suitable electrodes are available. Testing has been done to ensure that interferences are not a problem. The electrodes which we have found useful are CN^-, Cl^-, F^-, NO_3^-, Cu^{++}, Pb^{++}, NH_4^+ and S^{--}. Calibration curves for the Cu^{++}, Pb^{++}, NH_4^+ and S^{--} electrodes have been obtained and their linear ranges are given in Table XX.

Table XX

Ion	Linear Working Range
Cu^{++}	0.05 mg/ℓ to satd.
Pb^{++}	5×10^{-5} M to 1×10^{-1} M
NH_4^+	0.5 mg/ℓ to 1.4 gm/ℓ
S^{--}	0.01 mg/ℓ to 30 gm/ℓ

Appendix A

Preprint of a paper submitted to Analytical Chemistry on $MgCl_2$ interferences in lead analysis.

BRIEF

The interference of $MgCl_2$ on lead analysis is investigated and occlusion is shown to be a dominant interference. Atomization from a nonpyrolytic graphite surface reduces this interference.

A Study on the Mechanism of Interference of Magnesium Chloride on Lead Analysis in Graphite Furnace Atomic Absorption

J. P. Erspamer and T. M. Niemczyk*

The Department of Chemistry, The University of New Mexico,

Albuquerque, New Mexico 87131

ABSTRACT

The nature of a $MgCl_2$ matrix interference on the analysis of lead is investigated. The response of the lead absorption signal when atomized from a pyrolytic graphite surface is compared to that when atomized from a nonpyrolytic graphite surface. The results indicate that both chemical interactions and physical interactions, namely occlusion, are important when a pyrolytic graphite surface is used. The use of a nonpyrolytic graphite surface reduces the physical interference.

Lead is probably the most frequent analysis performed by flameless atomic absorption techniques. In ideal cases, flameless atomic absorption techniques are very sensitive for lead analysis, however, when real samples are analyzed many interferences are noted. The interference due to alkali and alkaline earth metal chlorides seems to be among the most troublesome and common. These metal chloride systems are unique in that they exhibit many different types of interferences. Although these systems have been extensively studied and numerous methods of interference control have been proposed, the physicochemical nature of some of the observed interferences is still not well understood.

Many studies have been performed on the lead-chloride system and several types of interferences have been reported (1-7). Vapor phase interactions resulting in the formation of molecular chlorides have been discussed (7-11) and the corresponding spectra have been measured (12). When molecular species are formed not only is the analyte lost as a molecular species, but the absorbance due to nonatomic absorption also increases. Background absorption up to 1.0 absorbance units can be compensated for with present background correctors but often the dynamic range of the background corrector is exceeded (13). Segar and Gonzalez (14) have reported that the background absorbance observed when a seawater matrix is present exceeds the range of a deuterium arc background corrector.

Frech and Cedergren (5) have found in a study of Pb in NaCl solutions that NaCl exhibits a nonatomic absorbance when ashed up to 1000 C. They also report that losses of lead are observed above 630 C in the presence of NaCl, however, no losses are observed up to 900 C in the absence of NaCl. This has been attributed to the formation of molecular chlorides and the covolatilization of Pb with alkali metals. Czobik and Matousek (2) have also reported a carrier effect when lead is present in a NaCl medium. In the presence of 2 mg of NaCl, the appearance

temperature of Pb is decreased significantly. This is attributed to the simultaneous introduction of Pb and NaCl into the optical path upon evaporation of the salt.

The presence of $MgCl_2$ has been reported as one of the more troublesome chloride matrices. Hodges (15) observed a depression in the lead absorption signal in the presence of 475 µg/ml $MgCl_2$. Fuller (5) reported the effect of 0.1% $MgCl_2$ on the lead absorbance. More recently, Manning and Slavin (1) reported a severe suppression of the Pb absorption signal in the presence of 4% $MgCl_2$ and investigated several methods of interference control.

The reason chloride matrices are so difficult to deal with lies in the fact that the volatilization temperature of many chloride salts is similar to that of lead. This prevents one from eliminating the matrix during the preatomization cycle and thus isolating the analyte prior to the atomization cycle. The result is a time overlap in the furnace between the analyte and the interferent during atomization. This time overlap gives rise to the formation of stable molecular species in the vapor phase, and consequently, the lead goes undetected. Further losses of lead are due to the volatilization of molecular lead chloride species that diffuse out of the furnace before thermal dissociation can occur.

Attempts have been made to resolve the similarity in volatilization temperature by altering the matrix volatility while leaving that of the analyte unchanged. Ediger (26) introduced the concept of matrix modification by adding NH_4NO_3 to a chloride matrix. This resulted in the formation of NH_4 Cl which volatilizes at 500 C, which is well below the atomization temperature of Pb. The use of various acids (8,15,16) and H_2(5) have also been employed to control the interference due to chloride. Presumably, HCl is formed and is swept out of the furnace prior to atomization.

The mechanism of atomization is not completely understood and is somewhat dependent on the analyte. In the case of lead, the mechanism proposed by Aggett and Sprott (17) and Campbell and Ottaway (18) involves the reduction of the analyte oxide by the furnace wall:

$$MO(s) + C(s) \rightarrow M + CO(g) \qquad (1)$$

The thermal dissociation of the oxides and chlorides of the analyte has also been considered:

$$MX \xrightarrow{\Delta} M + 1/2\ X_2 \qquad (2)$$

$$MO \xrightarrow{\Delta} M + 1/2\ O_2 \qquad (3)$$

Regan and Warren (7) and Fuller (6) have added water soluble organic compounds, such as oxalic acid, to reduce the interference observed when a chloride matrix is present. Presumably, this creates a molecular mixture of carbon and analyte which promotes the reduction of PbO to the less volatile free Pb.

The use of tubes coated with carbide-forming elements has been reported for determinations involving carbide forming analytes (19,20). It has been speculated that this blocks the active sites on the furnace wall by forming carbides with the protective agent and thus prevents the analyte from doing the same. More recently tube coatings have been employed for the analysis of Pb in chloride matrices (1,21). It is not clear at this time what effect this has on the lead-chloride system, however, it may be speculated that the reduction of PbO is somehow enhanced.

EXPERIMENTAL

A Varian Techtron model AA6 atomic absorption spectrophotometer was used in conjunction with a CRA-90 graphite furnace. The spectrophotometer was equipped with a BC-6 background corrector. All samples were introduced into the furnace using eppendorf pipets.

The lead absorption was monitored at the 217.0 nm line. The sample underwent the typical three-stage heating cycle beginning with drying at 100 C for 60 seconds, ashing at variable temperatures for 60 seconds and atomization at 2200 C with a 600°/sec ramp and a one hold time. All measurements were made in the peak height mode. The pulse shapes were monitored on a Techtronix model 5119 storage oscilloscope.

All solutions were made using reagent grade chemicals and distilled/deionized water. All laboratory glassware and plastic containers were washed and rinsed with 5% HNO_3 and further rinsed with distilled/deionized water. The nonpyrolytic graphite surface was obtained by sanding the pyrolytic coating off the standard tubes.

RESULTS AND DISCUSSION

Some insight into the fundamental nature of the interferences of chloride matrices on lead analysis can be gained by studying the kinetics of atom release in a qualitative sense by monitoring the absorbance peak shapes. As will be shown, the optimum experimental parameters and the kinetics of atom release vary when atomization takes place from pyrolytic and nonpyrolytic graphite.

Optimization of Experimental Conditions. In the early stages of the study, difficulties with the precision of the measurements were experienced. It has been noted in the literature that the addition of HNO_3 sometimes improves the precision.

The effect of HNO_3 was investigated and the results are shown in Fig. 1. At HNO_3 concentrations above 0.60 M, the Pb absorption is essentially constant. The improvement in precision is shown in Table I. On the basis of these results, the remainder of the experiments were carried out with a HNO_3 concentration of 0.60 M. Although higher concentrations of HNO_3 may improve the precision slightly and the interference due to higher concentrations of $MgCl_2$ may be more effectively reduced, the lifetime of the tube is decreased significantly due to the more corrosive atmosphere.

The influence of the ashing temperature on the Pb absorption signal was also investigated and the results are shown in Fig. 2. The optimum ashing temperature when using a pyrolytic graphite tube is 625 C. When a nonpyrolytic graphite tube is used, the optimum lies at 750 C. The ability to ash at a higher temperature enables one to eliminate more of the matrix before the onset of atomization. This reduces both the physical and vapor phase interactions caused by chloride during the atomization cycle. It is possible that the reduction of PbO takes place more efficiently on the nonpyrolytic graphite thus allowing one to employ a higher ashing temperature without significant losses of lead (22,23).

Interference Studies. Fuller (24) has proposed a kinetic approach to atomization that relates absorbance to several kinetic parameters:

$$\text{Absorbance (M)} = p\, M_o \frac{k_1}{k_2 - k_1} \left[\exp(-k_1 t) - \exp(-k_2 t)\right] \qquad (4)$$

where M_o is the initial amount of element introduced into the furnace, k_1 is the first order rate constant for atom formation, k_2 is the first order rate constant for atom removal and p is a constant related to the oscillator strength and the efficiency of metal atom production.

From the above equation, changes in the kinetics of the atomization processes will be reflected in changes in the shape of the absorbance vs. time profile. If

k_1 is decreased and k_2 and p are held constant, the peak absorbance will decrease, the time between the beginning of the absorbance pulse and the peak absorbance will increase, and the integrated absorbance will remain constant. If k_2 is decreased and k_1 and p are held constant, the peak absorbance will increase, the time between the beginning of the absorbance pulse and the peak absorbance will increase, and the integrated absorbance will increase. In this case, the peak appears larger in all dimensions with an increased integrated absorbance. Finally, if p is decreased and k_1 and k_2 are held constant, the peak absorbance will decrease and the time between the beginning of the pulse and the peak absorbance will decrease.

Figure 3 shows the absorbance vs. time profiles for Pb in the presence of varying amounts of $MgCl_2$ when atomized from a pyrolytic graphite surface. As the $MgCl_2$ concentration increases, one observes a change in the absorbance vs. time profile. First, the peak absorbance decreases significantly. Second, the time required to reach the peak absorbance increases with increasing $MgCl_2$ concentration and, finally, the onset of the peak is delayed. These are indicative of decreases in k_1, or indicative of a decrease in the rate of atom formation.

All of these results may be attributed to occlusion of the analyte by the salt matrix. The delay in the onset of the peaks may be due to a change in heating rate experienced by the analyte. If the analyte is entrained in clusters of matrix molecules, then a loss of thermal contact between the analyte and the furnace wall would be expected. Furthermore, if carbon does indeed play a major role in the reduction of the analyte oxide as has been proposed, then one would expect a decrease in the rate of reduction of the oxide due to the loss of contact between the furnace wall and analyte as a result of occlusion. The decrease in the rate of reduction, and hence a decrease in the rate of atom production, would be reflected as a decrease in k_1.

Figure 4 shows the absorbance vs. time profiles for Pb in the presence of varying amounts of $MgCl_2$ when atomized from a nonpyrolytic graphite surface. The first thing one notes is that the onset of the absorption peak is not delayed with increasing $MgCl_2$ concentration. Furthermore, the peaks retain their shape even though the peak height and peak area decrease. This could be the result of several effects. Electron micrographs (25) of pyrolytic and nonpyrolytic graphite surfaces have shown that the nonpyrolytic graphite has a much greater surface area. The increased surface area allows better contact between the analyte and the furnace wall. This reduces the physical interaction between the matrix and analyte through a dilution effect. Also, since the contact between the analyte and the graphite surface is increased, the analyte reduction step (reaction 1) should be enhanced on the nonpyrolytic graphite surface as opposed to the same step on the pyrolytic graphite surface. This is supported by the fact that the optimum ashing temperature is 125 C higher when the nonpyrolytic graphite surface is used. Finally, the retention of peak shape with increasing $MgCl_2$ concentration indicates that k_1 is not changing, however, the atomization efficiency is decreasing. The reduction of p, the atomization efficiency, is probably due to the formation of molecular chlorides in the vapor phase. These effects may be attributed to the higher reducing capacity of nonpyrolytic graphite over that of pyrolytic graphite.

To test this thesis, measurements were made on solutions that conatined Pb, $MgCl_2$ and 1% oxalic acid when atomized from both surfaces. The addition of oxalic acid should make a more reducing atmosphere in the furnace. One could expect to see the same trends as were observed on going from pyrolytic graphite to nonpyrolytic graphite when oxalic acid is added to the solution. Figure 5 shows the absorbance as a function of final ashing temperature in the presence of oxalic acid.

The optimum ashing temperature has increased in the presence of oxalic acid for atomization from both surfaces. Figures 6 and 7 show the absorbance vs. time profiles for Pb in the presence and in the absence of oxalic acid. Table II shows the enhancement due to the addition of oxalic acid.

When a pyrolytic graphite surface is employed the effect of oxalic acid is quite drastic. The peak absorbance is enhanced by factor of 3.7 and the time required to reach the peak absorbance is decreased by 16% in the presence of oxalic acid. This is indicative of an increase in both k_1 and p on going to a more reducing atmosphere. The effect of oxalic acid when the nonpyrolytic graphite tube is used is not as drastic as was seen when the pyrolytic graphite tube was used. Although the peak height is increased, the time required to reach peak absorbance remains essentially constant. This is reasonable since the nonpyrolytic graphite surface was quite reducing to begin with and, therefore, the change in reducing capacity with the addition of oxalic acid is not as great on the nonpyrolytic graphite surface as was seen in the case of the pyrolytic graphite surface.

The appearance temperature of Pb was measured for atomization from both pyrolytic and nonpyrolytic graphite and in the presence and absence of oxalic acid and the results are shown in Table III. Again, when the pyrolytic graphite tube is used there is a drastic change as the conditions are varied. There is an increase in appearance temperature on going from aqueous lead solutions to lead in the presence of $MgCl_2$ and finally an even greater increase in the presence of oxalic acid. The increase in the appearance temperature in the presence of $MgCl_2$ may be attributed to occlusion. When oxalic acid is present, the species being atomized is probably free Pb which is less volatile than either lead oxides or lead chlorides and, therefore, a higher temperature is required.

The appearance temperatures for the same solutions on nonpyrolytic graphite remain relatively constant for all three cases. This lends further support to the idea that the atomization processes are relatively unperturbed by the addition of a chloride matrix when a nonpyrolytic graphite surface is used.

Memory Effects. Memory effects due to the matrix have been observed. Figure 8 shows the response of an aqueous lead sample before and after a sample containing a high concentration of $MgCl_2$ was fired in the tube. The shift in time of the peak after a sample with a high salt concentration has been fired indicates a buildup of salt in the tube. This lends support to the idea that the heating rate is altered by the salt as was seen above. The peak shape is not significantly altered, however, the peak height is reduced which is probably due to the formation of molecular chlorides. If the tube is burned out at about 3000 C after the firing of a sample with a high salt concentration there is no memory effect observed. Furthermore, we did not under any circumstances observe a memory effect due to lead. The shift of the peak was not observed when the nonpyrolytic graphite tubes were used.

CONCLUSION

The Pb-$MgCl_2$ system seems to be an excellent model for interference studies since it exhibits most of the interferences that have been noted in the literature. Furthermore, its behavior is similar to many real samples such as biological systems, sea water and ground water. The results of this study indicate that control of the reducing properties of the furnace along with a careful consideration of the temperature program can minimize some matrix interferences. The use of nonpyrolytic graphite, in cases where carbide formation is not a problem, may also prove to be beneficial when a difficult matrix is present.

CREDITS

The work upon which this publication is based was supported in part by EPA Grant R806303010, New Mexico Energy and Minerals Department Project 78-3113 and by funds provided through the New Mexico Water Resources Research Institute by the United States Department of Interior, Office of Water Resources and Technology, as authorized under the Water Resources Research Act of 1964, Public Law 88-379, under project number 1423641.

REFERENCES

(1) D. C. Manning and W. Slavin, Anal. Chem., 50, 1234 (1978).

(2) E. J. Czobik and J. P. Matousek, Anal. Chem., 50, 2 (1978).

(3) W. Frech and A. Cedergren, Anal. Chim. Acta, 82, 93 (1976).

(4) K. Johansson, W. Frech and A. Cedergren, Anal. Chim. Acta, 94, 245 (1977).

(5) W. Frech and A. Cedergren, Anal. Chim. Acta, 88, 57 (1977).

(6) C. W. Fuller, Atomic Absorpt. Newslett., 16, 106 (1977).

(7) J. G. T. Regan and J. Warren, Analyst, 101, 220 (1976).

(8) C. W. Fuller, Anal. Chim. Acta, 81, 199 (1976).

(9) B. R. Culver and T. Surles, Anal. Chem., 47, 920 (1975).

(10) S. Yasuda and H. Kakiyama, Anal. Chim. Acta, 84, 291 (1976).

(11) J. B. Dawson and M. K. Kier, Analysis, 4, 273 (1976).

(12) S. Yasuda and H. Kakiyama, Anal. Chim. Acta, 89, 369 (1977).

(13) Instruction Manual, Model BC-6 Simultaneous Background Detector, Varian Techtron Pty. Ltd., Publication No. 85-100026-00, 4th Ed., May 1978.

(14) D. A. Segar and J. G. Gonzalez, Anal. Chim. Acta, 58, 7 (1972).

(15) D. J. Hodges, Analyst, 102, 66 (1977).

(16) A. Katz and N. Taitel, Talanta, 24, 132 (1977).

(17) J. Aggett and A. J. Sprott, Anal. Chim. Acta, 72, 49 (1974).

(18) W. C. Campbell and J. M. Ottaway, Talanta, 21, 837 (1974).

(19) R. Cioni, A. Mazzucotelli and G. Ottonello, Anal. Chim. Acta, 82, 420 (1976).

(20) J. H. Runnels, R. Merryfield and H. B. Fisher, Anal. Chem., 47, 1258 (1975).

(21) K. C. Thompson, K. Wagstaff and K. C. Wheatstone, Analyst, 102, 310 (1977).

(22) C. W. Fuller, Atomic Absorpt. Newslett., 16, 106 (1977).

(23) J. G. T. Regan and J. Warren, Atomic Absorpt. Newslett., 17, 89 (1978).

(24) C. W. Fuller, Analyst, 101, 798 (1976).

(25) R. E. Sturgeon and C. L. Chakrabarti, Anal. Chem., 49, 90 (1977).

(26) R. E. Ediger, At. Absorpt. Newslett., 14, 127 (1975).

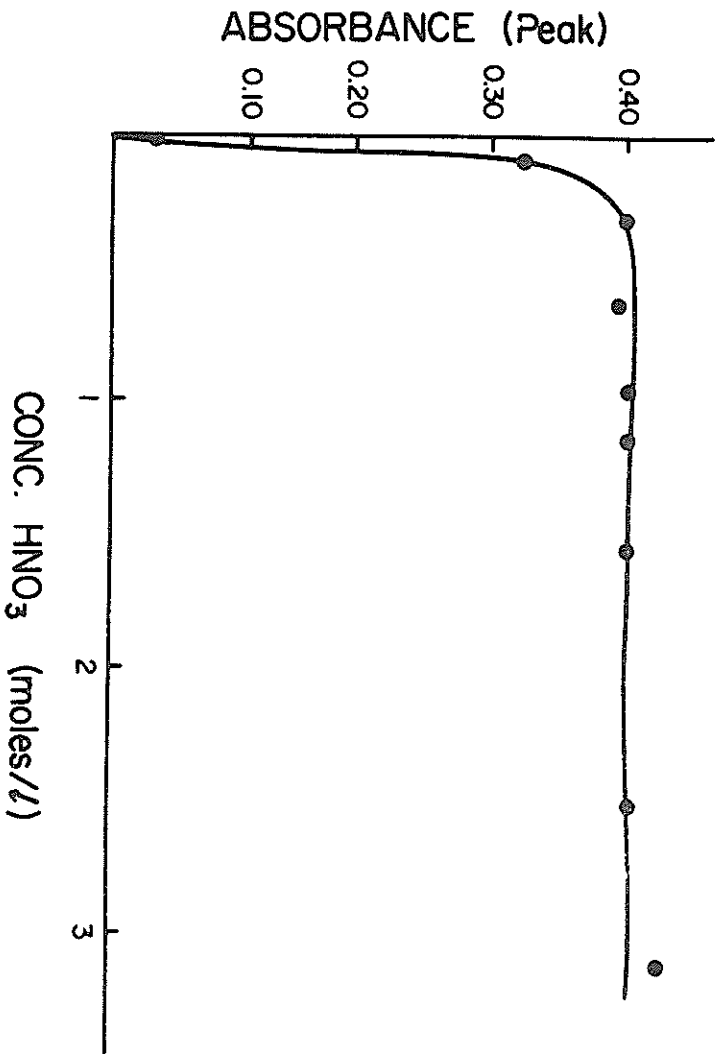

Figure 1. The effect of HNO_3 on a solution containing 0.4 ppm Pb and 10 $\frac{mg}{ml}$ $MgCl_2$.

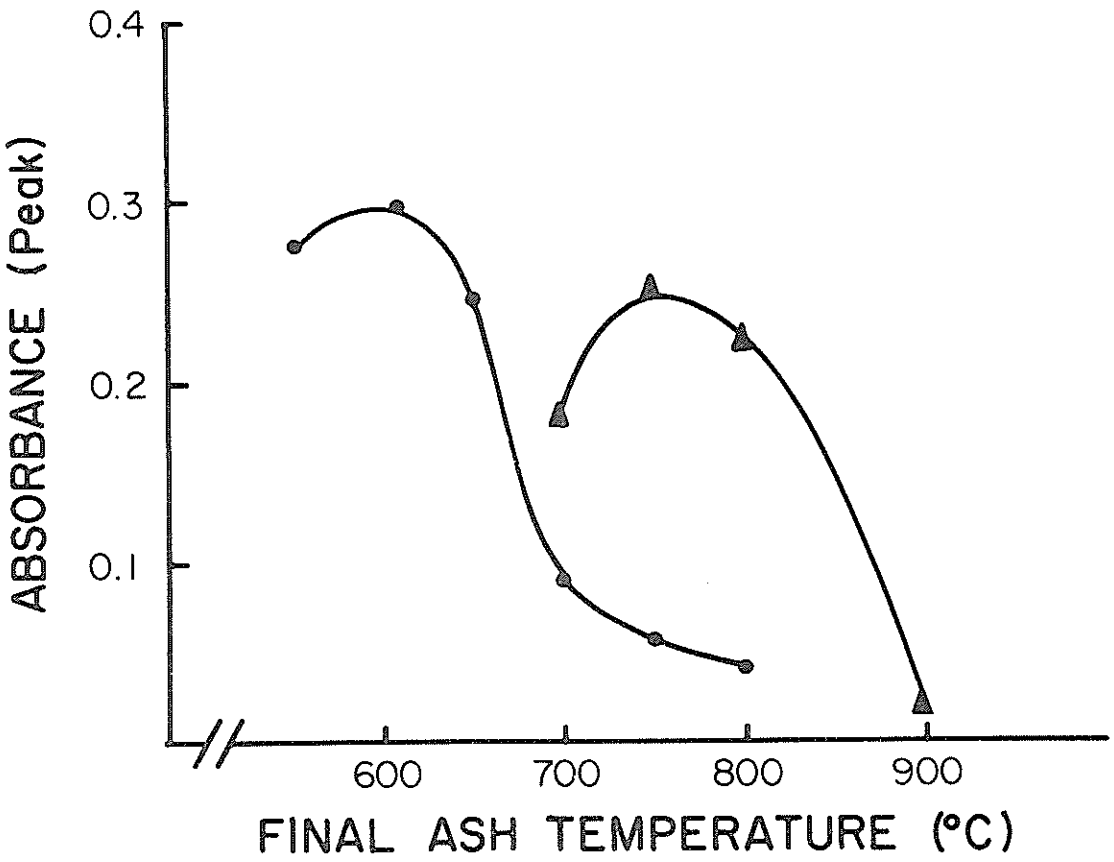

Figure 2. The peak absorbance as a function of final ash temperature for a solution containing 0.4 ppm Pb and 4.5 $\frac{mg}{ml}$ $MgCl_2$ when atomized from a pyrolytic graphite surface (○) and for a solution containing 0.4 ppm of Pb and 56 $\frac{mg}{ml}$ $MgCl_2$ when atomized from a nonpyrolytic graphite surface(△); ashing time: 60 seconds.

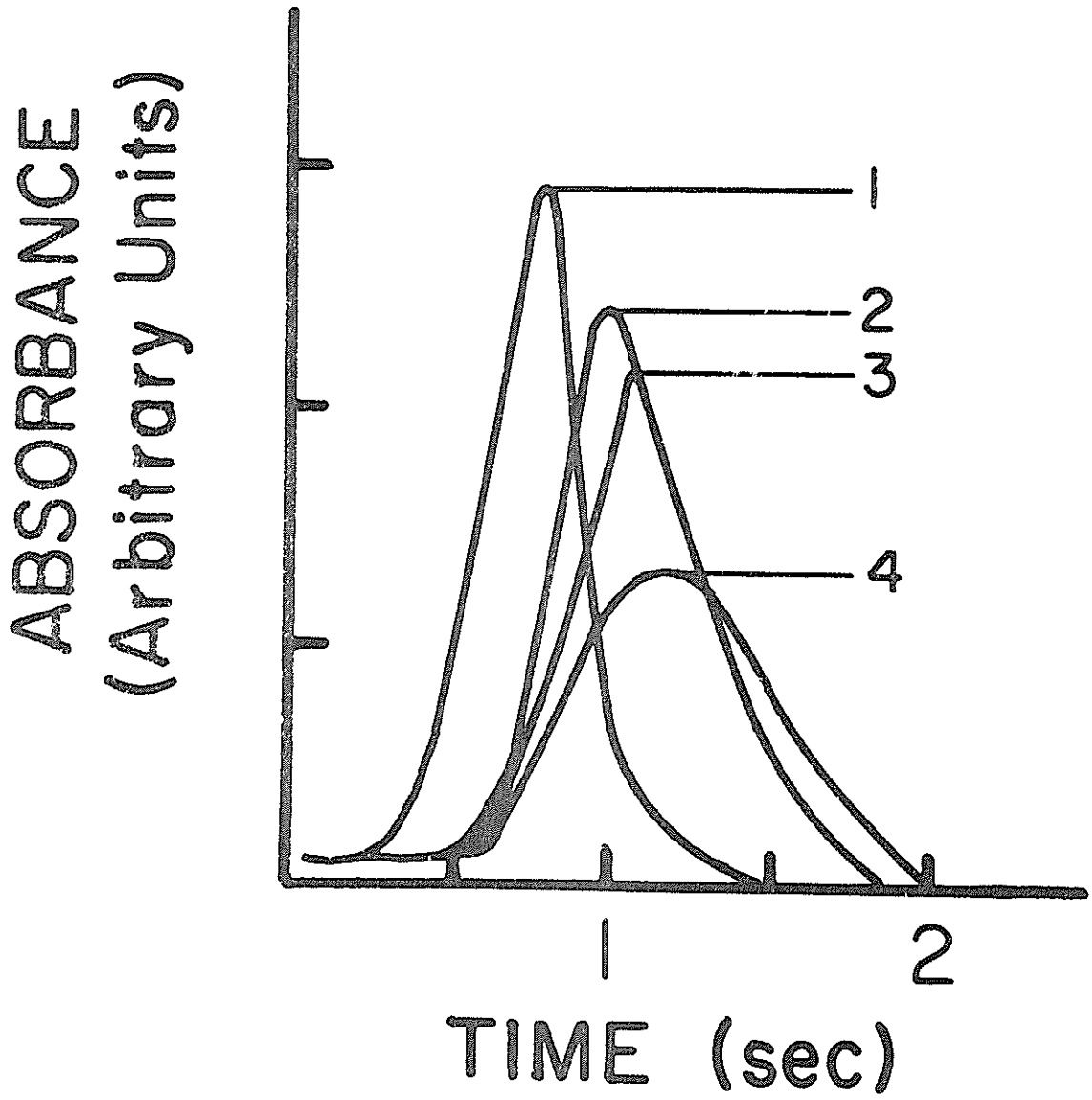

Figure 3. The absorbance vs. time profiles for a solution containing 0.4 ppm Pb and varying amounts of $MgCl_2$. (1) No $MgCl_2$. (2) 14 $\frac{mg}{ml}$ $MgCl_2$. (3) 28 $\frac{mg}{ml}$ $MgCl_2$. (4) 84 $\frac{mg}{ml}$ $MgCl_2$.

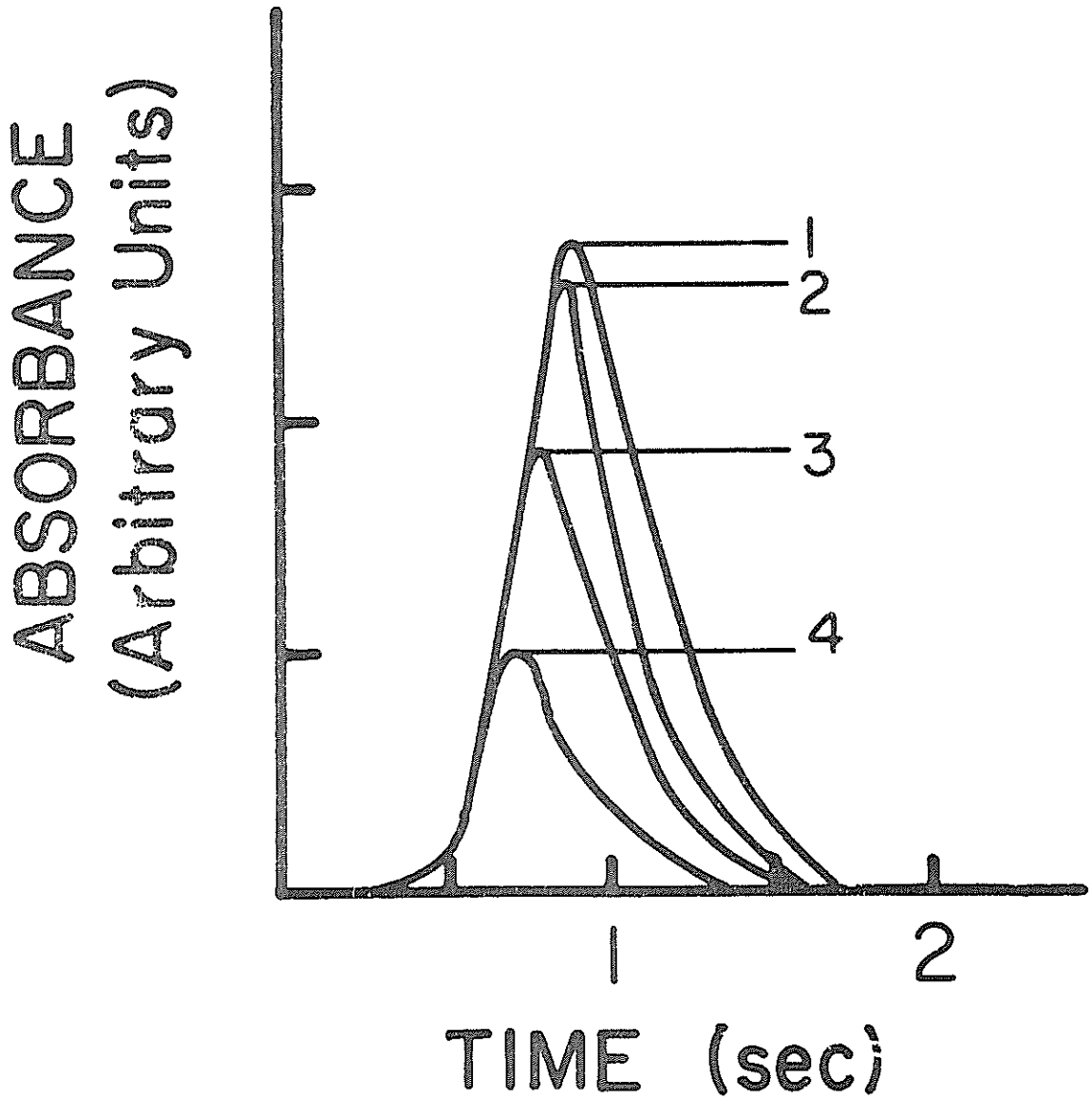

Figure 4. The absorbance vs. time profiles for a solution containing 0.4 ppm Pb and varying amounts of $MgCl_2$ when atomized from a nonpyrolytic graphite surface. (1) No $MgCl_2$. (2) 14 $\frac{mg}{ml}$ $MgCl_2$. (3) 28 $\frac{mg}{ml}$ $MgCl_2$. (4) 84 $\frac{mg}{ml}$ $MgCl_2$.

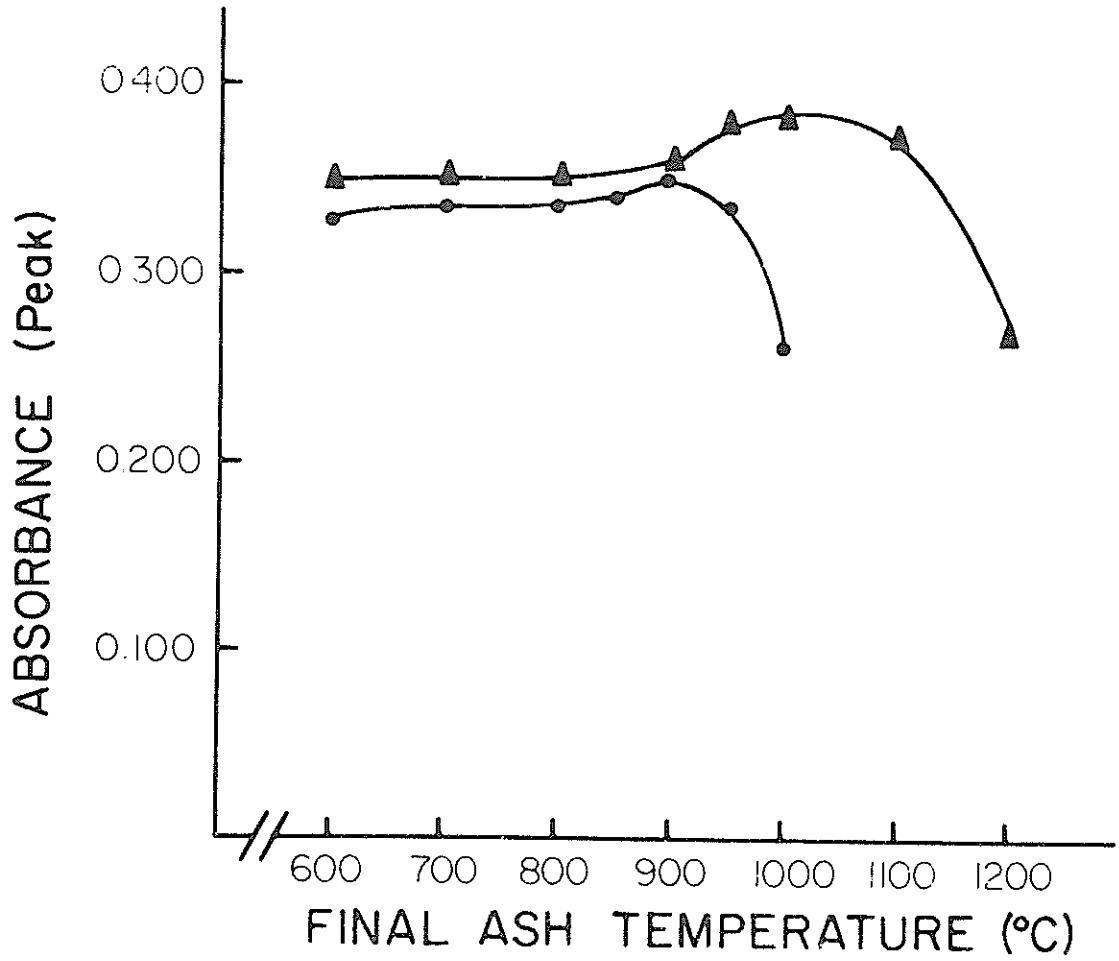

Figure 5. The peak absorbance as a function of final ashing temperature for a solution containing 0.2 ppm Pb, 7 $\frac{mg}{ml}$ $MgCl_2$ and 1% oxalic acid when atomized from a pyrolytic graphite surface (Δ) and a nonpyrolytic graphite surface (O).

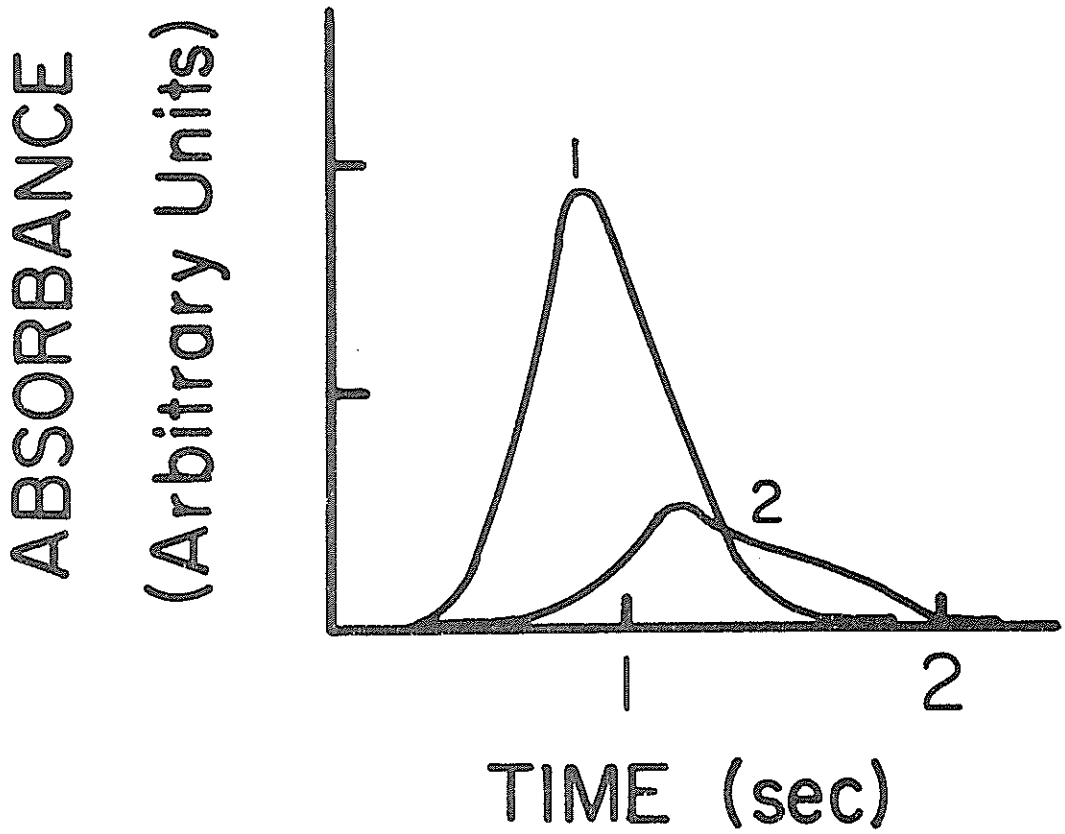

Figure 6. The absorbance vs. time profile for a solution containing (1) 0.2 ppm Pb, 28 $\frac{mg}{ml}$ $MgCl_2$ and 1% oxalic acid and (2) 0.2 ppm Pb and 28 $\frac{mg}{ml}$ $MgCl_2$ when atomized from a pyrolytic graphite surface. Temperature program: (1) Dry: 100 C, 60 seconds; Ash: 625 C, 60 seconds; Atomize: 2200 C; (2) Dry: 100 C, 60 seconds; Ash: 1000 C, 60 seconds; Atomize: 2200 C.

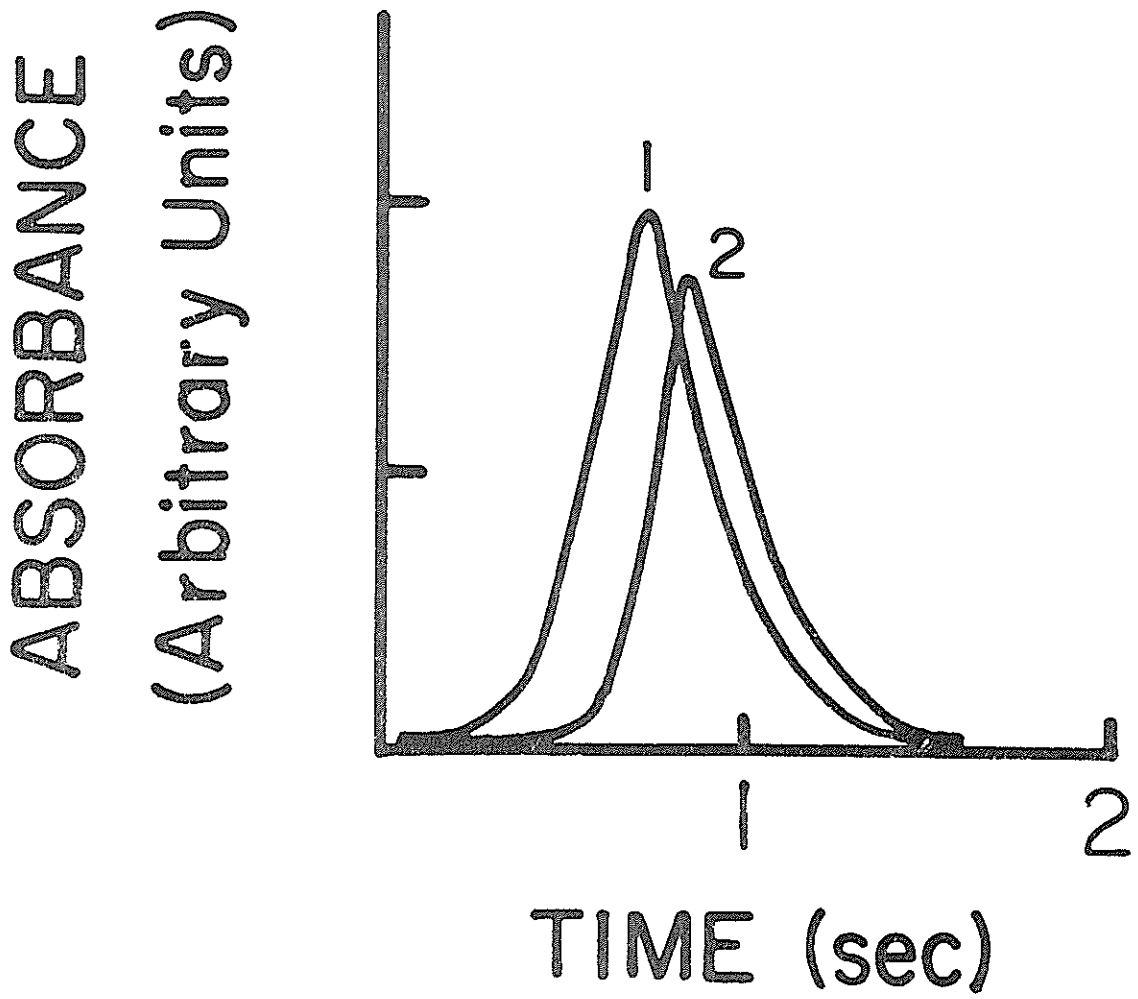

Figure 7. The absorbance vs. time profile for a solution containing (1) 0.2 ppm Pb, 28 $\frac{mg}{ml}$ $MgCl_2$ and 1% oxalic acid and (2) 0.2 ppm Pb and 28 $\frac{mg}{ml}$ $MgCl_2$ when atomized from a nonpyrolytic graphite surface. Temperature program: (1) Dry: 100 C, 60 seconds; Ash: 750 C, 60 seconds; Atomize: 2200 C; (2) Dry: 100 C, 60 seconds; Ash: 900 C, 60 seconds; Atomize: 2200 C.

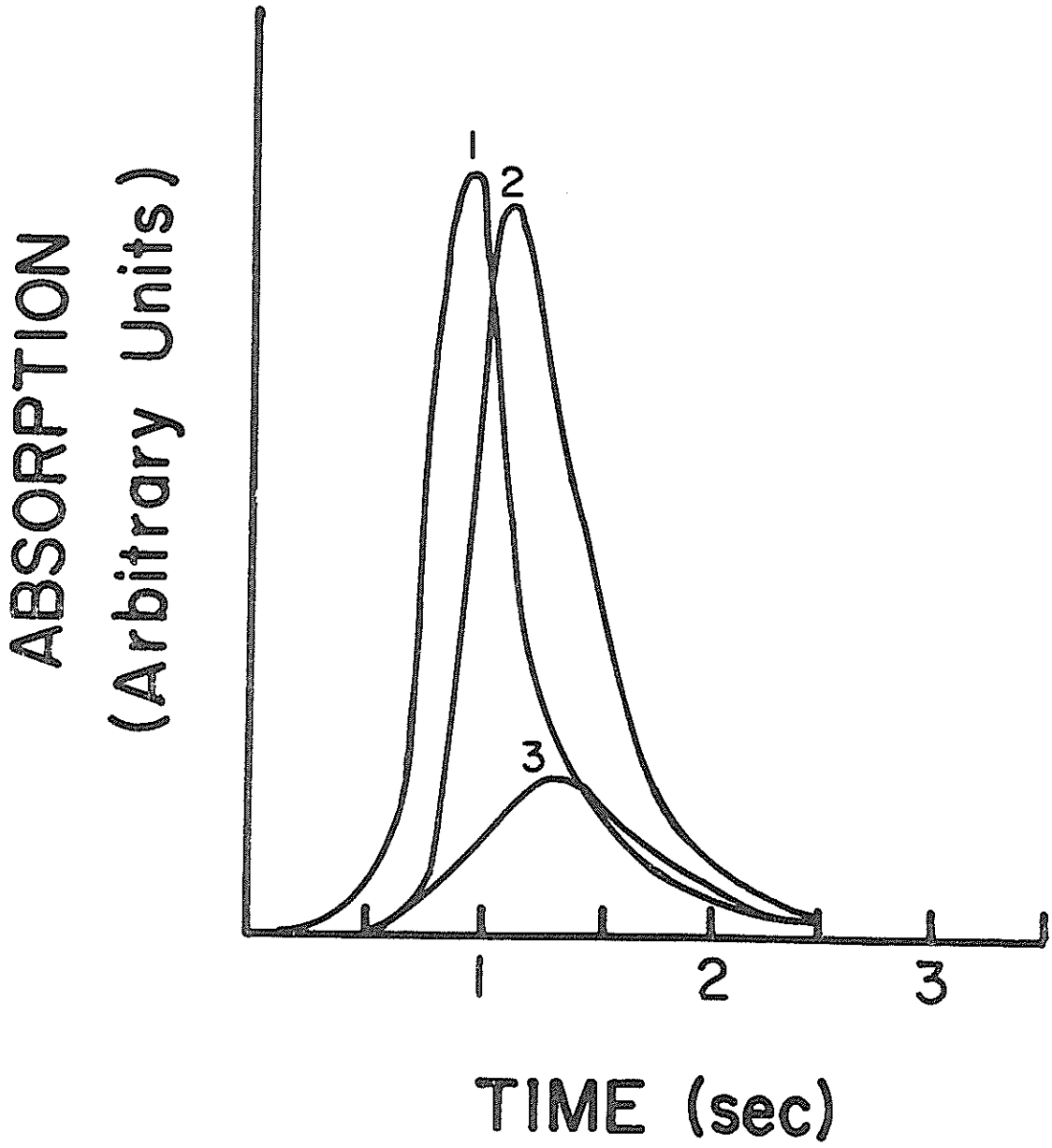

Figure 8. The memory effect due to the $MgCl_2$ matrix. Curves 1 and 2 correspond to a 0.4 ppm aqueous Pb solution, curve 3 is a solution containing 0.4 ppm Pb and 34 $\frac{mg}{ml}$ $MgCl_2$.

TABLE I

The Effect of HNO_3 on the Precision of Analysis

HNO_3 (Moles/l)	Standard Deviation (Absorbance Units)	Relative Standard Deviation
0	6.02×10^{-3}	22.8%
0.314	6.25×10^{-3}	1.56%
0.628	5.87×10^{-3}	1.48%
0.942	3.68×10^{-3}	0.91%
1.26	3.68×10^{-3}	0.91%
1.57	2.36×10^{-3}	0.58%
2.51	1.22×10^{-3}	0.30%
3.14	8.58×10^{-3}	2.0%

TABLE II

The Effect of Oxalic Acid on the Peak Absorbance

Solution	Peak Absorbance	
	Pyrolytic Graphite	Nonpyrolytic Graphite
0.4 ppm Pb	0.421	0.429
0.4 ppm Pb, 1% oxalic acid	0.411	0.443
0.2 ppm Pb, 28 mg/ml $MgCl_2$	0.072	0.267
0.2 ppm Pb, 28 mg/ml $MgCl_2$, 1% oxalic acid	0.294	0.299

TABLE III

Appearance Temperatures

Solution	Appearance Temperature (°C)	
	Pyrolytic Graphite	Nonpyrolytic Graphite
0.4 ppm Pb	950	1200
0.4 ppm Pb, 14 mg/ml $MgCl_2$	1175	1200
0.4 ppm Pb, 14 mg/ml $MgCl_2$, 1% oxalic acid	1265	1100

APPENDIX B

By

H. E. Nuttall, E. A. Walters, and T. M. Niemczyk

Published in

Proceedings of the Fifth Underground Coal Conversion Symposium,

Alexandria, VA, June, 1979

HYDROLOGIC AND ENVIRONMENTAL FINDINGS: SAN JUAN UCC SITE

H. E. Nuttall
Department of Chemical and Nuclear Engineering
University of New Mexico
Albuquerque, New Mexico 87131

E. A. Walters and T. M. Niemczyk
Department of Chemistry
University of New Mexico
Albuquerque, New Mexico 87131

ABSTRACT

In 1978, field and laboratory studies were initiated to assess the technical feasibility of underground coal gasification in the Fruitland coal field located in northwest New Mexico. Participants in the project include University of New Mexico, Public Service Company of New Mexico, Los Alamos Scientific Laboratory and Science Applications, Inc. A site has been selected and preliminary characterization has begun. Field activities include coring, logging, hydrologic testing and water sampling. Laboratory studies have been initiated to measure the distribution overburden, underburden and coal ion exchange constants for selected ions. The results from these activities are reported along with the laboratory analysis of water samples from both the underground coal conversion site and throughout the region. Extensive hydrologic studies of the entire region are being performed by the Bureau of Land Management and the U.S. Geological Survey to assess the nature and availability of water in this region to aid energy development. These regional findings will also be discussed and their impact on underground coal conversion assessed.

Introduction

The San Juan coal deposit in northwestern New Mexico has been recognized for several years as a strategic energy source for the future development of the southwest sun belt.[1,2,3] This coal supplies energy to several power plants which in turn serve the entire region and several new power plants have been proposed. Also, northwestern New Mexico was considered for the location of several large above-ground synthetic natural gas (SNG) plants. Technically, these SNG plants are still viable, though coal leasing problems have delayed their development. The San Juan coal is continually considered in the energy development of the southwest, and most of the strip mineable coal has been leased.

Because of the heavy demand on the strippable San Juan coal and the fact that over 90% of this deposit lies below the current 250-ft. strip mineable level, future coal based energy development must look to the immense resource of deep coal. This point is further emphasized by the data in Table I.[4] The deep coal in New Mexico is estimated to represent 4,750 quads of energy while the total energy from all fossil sources is estimated at 5,065 quads. Thus the deep coal constitutes about 94% of New Mexico's available fossil energy that could be considered for future energy growth. Even if only 50% of the deep coal is recoverable, there would be 2,400 quads of deep coal energy versus 300 quads from all other fossil energy sources.

To make this deep coal resource economically viable as a future energy source, the University of New Mexico, in cooperation with the Public Service Company of New Mexico and Los Alamos Scientific Laboratory, is studying the feasibility of underground coal gasification (UCG) for the San Juan basin of New Mexico. A field and laboratory project is ongoing. The project objectives and chosen site were discussed at the 4th UCC Symposium.[3] The material presented in this paper summarizes the hydrological and environmental findings resulting from ongoing UCG studies.

TABLE I

Fossil Energy Reserves: New Mexico
(estimated reserves in quads)

Natural gas, conventional formation	12
Methane from coal seams	45
Crude oil, conventional formations	3
Oil from tar sands	1
Crude oil, enhanced recovery	4
Coal, strip mineable	250
Coal, below strip mine level	4,750
	5,065

Estimates for conventional oil and gas resources from New Mexico Energy and Minerals Department.

Hydrogeology

The hydrology of the San Juan basin has been and is the subject of numerous studies.

Since an adequate water supply is essential to the development of the energy resources in this region, there is considerable interest in the hydrology of the area. The potential aquifers have been well identified, and maps have been prepared showing depth to top and total thickness of these possible aquifers.[5] From many years of oil and gas exploration in this area, hundreds of holes and corresponding cores and logs were available to prepare the detailed stratigraphic maps. The basin covers about 30,000 mi^2 in northwestern New Mexico and southwestern Colorado (Fig. 1). A brief description of the coal formations was given by Walters and Nuttall.[1] The San Juan basin is somewhat arbitrarily subdivided into 19 separate coal fields. Two basic coal formations are recognized, i.e., the Fruitland and Menefee formations.

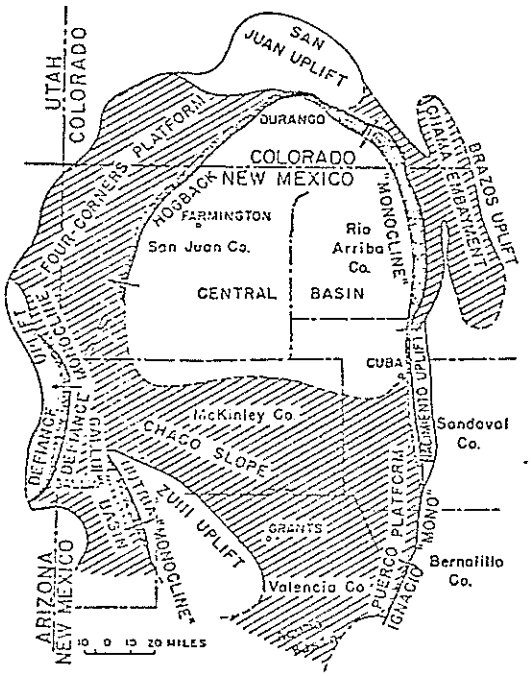

Figure 1. Location and structural elements of the San Juan basin (as modified from Kelley, 1951, by Beaumont and others, 1976).

The Fruitland coal is of primary interest in this study. The coal beds are highly lenticular, a consequence of their formation from peats at the edges of cretaceous swamps and estuaries. The surround rock is a wide variety of coastal sedimentary deposits, for example, sandstones, shales, siltstones and limestones. The coal seams are frequently infiltrated with fine layers of clays or other sedimentary deposits. The coal is a shrinking, highly volatile subbituminous coal that is very similar to the Hanna, Wyoming, coal.

The time-stratigraphic framework of the San Juan basin, including the coal rich Fruitland formation and the various potential aquifer formations, is presented in Fig. 2. Potential aquifers begin with the San Jose formation lying at the surface and extend to the deep Morrison formation.

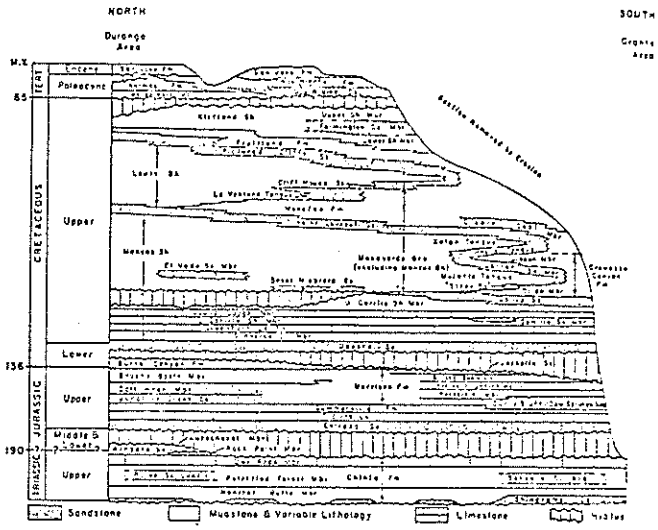

Figure 2. Time-stratigraphic framework and nomenclature, Triassic through Tertiary, San Juan basin (modified from Molenaar, 1977)

The Picture Cliffs sandstone is a potential aquifer of some interest since it underlies the Fruitland formation and the Fruitland coal seams. Unpublished data provided by the U.S. Geological Survey indicate that the Picture Cliffs sandstone is of very low permeability (<0.1 md) while the coal seams have a permeability of about 10 md.[3] Also from preliminary, potential flow maps for the Picture Cliffs sandstone in an area near the proposed San Juan underground coal conversion (UCC) site, the water migration rate appears to be 1-2 ft. per year; thus, very little water movement is observed in this formation. Above the Fruitland formation is the Kirtland shale. This formation also has very low permeability ($\sim$ 0.01 md). Thus it appears that the Fruitland coal is surrounded by formations of low permeability. It should be noted, however, that the deep Fruitland coal seams are water-saturated and well below the water table, which averages between 100-150 ft. below the ground surface. Consequently, the seams must be dewatered prior to gasification; however, at this time, it appears that the problems of too much water, as found at several of the western UCG test sites, will not be present in the development of UCG in the San Juan basin.

Environmental Studies

Baseline studies of the coal, overburden, underburden and groundwater are being conducted to assist in an evaluation of the environmental impact of UCG. Of particular concern and interest are concentrations of a selected set of metal ions, anions and organics. Laboratory experiments are being carried out to determine absorption and ion exchange constants for these species in order to provide data needed to construct a reasonable model of the site. Laboratory studies of ash leaching are also in progress.

Cores were taken from above the coal seam, through the coal and into the underburden for both wells. Descriptions of the cores are given in Tables II and III, and the site stratigraphy is illustrated in Fig. 3. Proximate and ultimate analyses of the coal were conducted for samples taken at 6-in. intervals across the principal seam. This included a stringer at a depth of about 500 ft. The results of these analyses on a moisture-free basis are given in Table IV. The results are typical of Fruitland formation coal; although the heating values are high enough to formally qualify it for a bituminous coal rank, both the percent fixed carbon and the nonagglomerating characteristics identify it as subbituminous A or B coal. There is a substantial amount of ash present, the maximum falling clearly at the location of the parting. The amount of sulfur in the coal again is typical of San Juan basin coal, lying in the range of 0.50-0.80%.

TABLE II

Core Description Versus Depth for GT-1

From (ft.)	To	Material
480.0	483.6	shiny gray, hard
483.6	484.0	core loss
484.0	492.4	shiny gray, hard, sandy bottom, 1.2 ft.
492.4	492.5	core loss
492.5	495.8	shiny gray, hard, silty
495.8	498.95	coal, medium bright, hard, fractured, resinous
498.95	499.25	shiny, black, carbonaceous
499.25	499.85	coal, dull, hard, very shaley
499.85	500.80	shiny black, hard
500.80	502.5	coal, dull, fractured
502.5	504.2	coal, medium bright, hard
504.2	504.7	shiny black, carbonaceous, sandy at top; coal, medium bright, hard

TABLE II (continued)

From (ft.)	To	Material
506.4	506.8	shiny black, hard, carbonaceous, light tan silty band 0.02 at bottom and 0.10 from top, mixed with coal
506.8	511.2	coal, medium bright, hard, resinous
511.2	511.3	shiny, light tan, hard
511.3	512.5	coal, medium bright, hard, resinous
512.5	517.2	coal, medium bright-bright, hard, resinous
517.2	518.3	shiny gray, hard
518.3	522.0	siltstone, gray, very hard, interbedded with thin SS lenses

TABLE III

Core Description Versus Depth for GT-2

From (ft.)	To	Material
470	474	shale gray, hard
474	474.5	shale gray, hard with sandstone veins
474.5	476.0	shale gray, hard with coal inclusions
476.0	480.0	core loss
480	486.6	shale, gray, moderately firm, sandy, sandstone stringers, coal inclusions
486.6	488.0	shale gray to dark gray, moderately firm to firm
488.0	490.0	shale gray to dark gray, moderately firm to firm
490.0	491.0	shale gray to dark gray, firm, sandy (small stringer of coal at 491.0)
491.0	495.5	sandstone-light gray, hard, fine to medium grained, carbonaceous stringers
493.5	494.7	core loss
494.7	496.0	shale, gray, moderately firm to firm, somewhat sandy
496.0	501.7	shale gray to dark gray, firm to very firm, somewhat sandy, carbonaceous inclusions
501.7	502.6	carbonaceous shale gray, sandy, sandstone stringers
502.6	502.8	carbonaceous shale light brown, firm, sandy, highly carbonaceous
502.8	504.0	coal black, hard, dull, pyrite, resinous (one thin sandstone stringer)
504.0	508.1	coal black, hard, dull, pyrite on fractures, resinous
508.1	508.3	carbonaceous shale dark gray, firm, highly carbonaceous

TABLE III (continued)

From (ft.)	To	Material
508.3	508.7	sandstone-brown, soft, medium to coarse-grained
508.7	510.7	coal black, hard, dull, pyrite, resinous
510.7	510.9	sandstone-brown to dark brown, fine-grained, firm, carbonaceous
510.9	514.0	coal black, dull, hard, pyrite with resin
514.0	515.8	coal black-dull, hard and brittle, pyrite and resinous
515.8	517.1	carbonaceous shale-dark brown (inclusions of coal), highly carbonaceous
517.1	518.2	shale, gray, firm, sandy
518.2	519.0	core loss

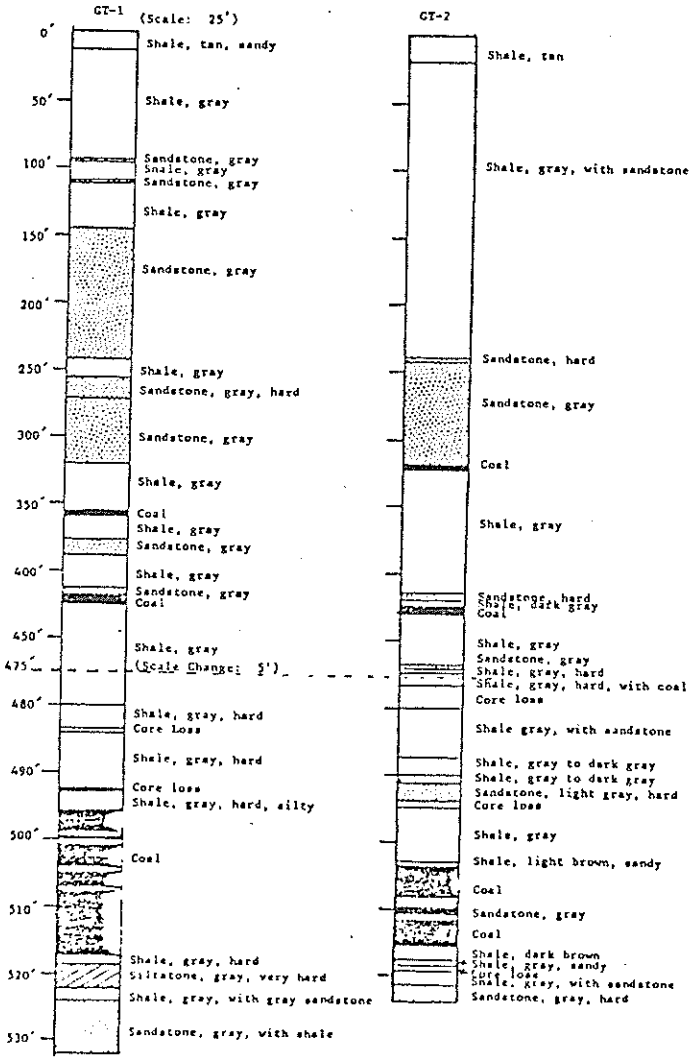

Figure 3. Stratigraphy of the San Juan UCG test site

TABLE IV

Geochemical Properties of the GT-1 Core Versus Depth (moisture-free basis)

Sample No.	Depth (Ft.)	C	H	O	N	S	Ash	Btu/lbm	Volatile	Fixed Carbon
33	496.0-496.5	68.69	5.16	11.75	1.19	0.87	12.76	11253	42.34	45.90
34	496.5-497.0									
35	497.0-497.5	72.07	5.37	11.69	1.72	0.87	9.57	12967	42.62	48.81
36	497.5-498.0									
37	498.0-498.5	71.48	5.19	12.48	1.81	0.71	9.33	12788	42.20	48.46
38	498.5-499.0									
39	499.0-499.5	34.78	2.41	9.62	0.57	1.85	51.62	5459	23.76	24.62
40	499.5-500.0									
41	500.0-500.5	12.97	1.16	3.48	0.29	2.89	76.89	1965	13.15	9.96
42	500.5-501.0									
43	501.0-501.5	55.29	4.30	14.59	1.46	0.94	27.31	9840	36.97	35.72
44	501.5-502.0									
45	502.0-502.5	44.76	3.83	7.99	1.31	3.34	40.66	7952	38.13	31.77
46	502.5-503.0									
47	503.0-503.5	47.72	3.84	9.97	1.33	0.78	36.78	8461	36.46	32.82
48	503.5-504.0									
49	504.0-504.5	39.36	3.38	12.27	1.03	0.82	44.19	6731	27.48	28.34
50	504.5-505.0									
51	505.0-505.5	72.80	5.23	11.34	1.77	0.66	8.16	12777	44.75	47.05
52	505.5-506.0									
53	506.0-506.5	70.38	5.28	10.38	1.72	0.64	10.60	12514	41.22	48.18
54	506.5-507.0									
55	507.0-507.5	61.31	4.66	11.17	1.15	0.56	20.15	10983	37.79	42.06
56	507.5-508.0									
57	508.0-508.5	71.51	5.18	13.34	1.69	0.38	9.37	12672	41.76	49.87
58	508.5-509.0									
59	509.0-509.5	72.37	5.22	12.33	1.86	0.84	8.78	12867	41.83	49.39
60	509.5-510.0									
61	510.0-510.5	72.44	5.56	11.68	1.65	0.37	8.71	12940	42.82	48.21
62	510.5-511.0									
63	511.0-511.5	53.87	4.51	10.71	1.51	0.56	26.84	9939	36.73	36.43
64	511.5-512.0									
65	512.0-512.5	58.11	4.97	10.71	1.84	0.51	24.35	10419	38.78	36.73
66	512.5-513.0									
67	513.0-513.5	44.87	4.00	10.48	1.28	0.44	37.13	8165	32.42	30.42
68	513.5-514.0									
69	514.0-514.5	71.63	5.29	12.03	1.79	0.31	9.63	12707	42.84	46.63
70	514.5-515.0									
71	515.0-515.5	73.76	5.77	10.73	1.88	0.49	7.36	13328	46.34	46.33
72	515.5-516.0									
73	516.0-516.5	71.73	5.44	11.44	1.66	0.39	8.74	12953	42.97	48.29

X-ray diffraction, thin-section petrographic, and air permeability and porosity tests were made on overburden and underburden. The results are reported in Table V. In both cases, the rock is composed almost entirely of quartz, feldspar and clay. Clays make up almost 30% of the rock; the principal clay minerals are kaolinite and montmorillonite. (The large quantity of clay in the overburden particularly is significant for the self-cleaning of groundwater that becomes contaminated as a result of UCG since clays are good, natural ion exchangers.) For finely ground samples of overburden and underburden cation exchange capacities of 2.7 meq/100 g clay and 2.2 meq/100 g clay, respectively, were determined. Thus, there is potentially a very large sink for cations that complex with clays more strongly than the naturally dominant ions Na^+ and Al^{++}.

TABLE V

Physical and Thermal Properties of the Over- and Underburden From the GT-1 Core

Property / Sample #	Overburden 28		Underburden 80	
Permeability (md)	0.017		0.014	
Porosity (%)	8.1		7.7	
Minerals	Whole Rock	Clay (28%)	Whole Rock	
Quartz (%)	47		45	
Feldspar	25		26	
Kaolinite/chlorite	17	49	14	
Illite/Mica		5	2	
Montmorillonite	11	45	13	

The amounts of several metal ions that may be leached from 10 g of powdered overburden and underburden into 100 ml of unbuffered deionized water are given in Table VI. The final pH values of the solutions are also reported. The natural buffer effect of the rock is quite evident from these results. It is also apparent that the majority of leachable cations are Al^{+3}, Na^{+} and Fe^{+3}. Studies on the levels of these and the other ions in the rock are in progress.

TABLE VI

Metal Ion Concentrations Leached From Samples of Over- and Underburden

Ion, C	Overburden [C], ppm	Underburden [C], ppm
(pH-final	10.05	10.10)
Fe^{+3}	9.72	6.67
Mn^{+2}	0.2	0.1
Pb^{+2}	0.2	0.1
Zn^{+2}	0.042	0.055
Ca^{+2}	0.66	0.20
Sr^{+2}	0.0	0.0
Al^{+3}	45.	46.
Na^{+}	77.0	61.1
Ni^{+3}	0.04	0.04
Cu^{+2}	0.0004	0.0002

In another experiment, 5 g of powdered underburden were added to 100 ml of a solution whose pH had been adjusted to a predetermined value by the addition of HNO_3 or NaOH. After equilibrium was reached, the concentrations of several anions and total dissolved solids were determined. The results are reproduced in Table VII. Interestingly, all the solutions come to a final pH of 7.20 due to the buffer action of the rock. The data show increased solubility for the anions at both ends of the acidity scale with minima occurring in the vicinity of pH7. Quite clearly, the dominant anion is SO_4=.

TABLE VII

Anion Concentrations in Leachates from Underburden Samples

Initial pH	Total Dissolved Solids (g/10 ml)	[C], ppm	[F], ppm	[CN], ppm	[SO_4=], ppm
1.05	0.156	0.753	0.37	0.021	653.
2.08	0.026	0.623	0.12	0.028	436.
3.03	0.016	0.653	0.18	0.028	462.
4.04	0.009	0.643	0.21	0.027	444.
5.02	0.008	0.643	0.19	0.024	425.
6.01	-	0.623	0.20	0.013	481.
7.01	0.007	0.623	0.20	-	424.

TABLE VII (continued)

Initial pH	Total Dissolved Solids (g/10 ml)	[C], ppm	[F], ppm	[CN], ppm	[SO_4=], ppm
8.01	-	0.663	0.20	0.012	443.
9.02	0.007	0.633	0.20	-	436.
10.02	-	0.653	0.20	0.011	398.
11.00	0.009	0.653	0.21	-	558.
12.05	0.017	0.653	0.39	0.010	434.

Additional thin sections of typical overburden, underburden and parting sections have been prepared, and the following qualitative observations can be made:

- -Horizontal stratification is evident from vertical sections.
- -The minerals are extremely fine-grained. The grains are not apparent at a magnification of 35 X.
- -A good deal of fracturing has occurred at some point in the history of the sediment, but the pores have since filled with calcite and/or gypsum.
- -The fine-grained regions are highly compacted and exhibit low porosity.
- -Grains of quartz are clearly seen at a magnification of 35 X.
- -There is considerable organic content in this rock. In some sections, plant parts are clearly visible with minor disruption due to mineral intrusion.

Water samples have been collected from both wells using a sampling device which permits sample collection at any specified level. Samples were collected above the coal seam, in the coal seam and to a very limited extent below the coal. The water has been analyzed for a variety of species. The metal ion concentrations of a sample collected at 490 ft. from the ground surface are given in Table VIII. These results tend to parallel the leaching data from overburden and underburden with some significant exceptions.

TABLE VIII

Metal Ion Concentrations of Groundwater at a Depth of 490 Ft.

Ion	[C], ppm
Na^{+}	1380
K^{+}	14.5
Mg^{+2}	0.42
Ca^{+2}	1.3
Sr^{+2}	0.2
Zn^{+2}	0.014

TABLE VIII (continued)

Ion	[C], ppm
Si^{+4}	11
Cr^{+3}	0.000
Cu^{+2}	0.005
Cd^{+2}	0.001
Co^{+3}	0.002
Fe^{+3}	0.036
Mn^{+2}	0.000
Pb^{+2}	0.070
Be^{+2}	0.000

Results of analyses for a variety of anions in the same well are given in Table IX. There is a remarkable disparity in the chloride ion concentrations found in the groundwater compared to what can be leached from either overburden or underburden. The reason for this difference is not clear. Neither NO_3^- nor NO_2^- was detectable in the well. The water is highly mineralized, and very hard as can be seen from the TDS and alkalinity results.

TABLE IX

Anion Concentrations of Groundwater at a Depth of 490 Ft.

Ion	[C], ppm
CN^-	0.0063
F^-	2.56
Cl^-	1500
NO_3^-	<0.1
NO_2^-	<0.1
$SO_4^=$	812
$PO_4^{\equiv}$ (total)	0.17
$PO_4^{\equiv}$ (ortho)	0.26
$S^=$	22.8
TDS	3918 mg/l
Alkalinity	1724 ppm Ca CO_3
COD	none detectable
pH	9.25
Conductance	4.92 mMHO

Studies are currently underway on metal ion concentrations in coal and surrounding rock, metal concentrations of ash, baseline for organics in water, and absorption and ion exchange constants of the ions. We are also initiating a series of leaching studies from coal and ash prepared in several different ways to determine what can be leached by water and at what rates.

Conclusions

In this study to determine the technical suitability of San Juan coal seams for underground gasification, a stepwise approach is being followed. Two of the key factors (hydrology and environmental aspects) were reported on. Though the project is ongoing, the following observations can be presented subject to future findings.

Site Hydrology

- -The Fruitland coal has about a 10 md natural permeability. This is comparable to that measured for the Hanna, Wyoming, UCG tests.
- -The surrounding formations are low permeability clays (~0.01 md).
- -No significant aquifers either above or near the seam are believed to exist.

Environmental Aspects

- -The natural groundwater is low quality (high in dissolved minerals, >3000 ppm).
- -The surrounding clay is a good ion absorber (capacity ~ 2.5 meq/100 gm).

Findings to date for the successful application of the link vertical well-UCG technology are most positive and encouraging. Future flow logging and tracer tests scheduled for this summer will address and hopefully answer the important questions about the natural seam flow patterns. If these tests are positive and other considerations are positive, the next step would be small scale field burns.

References

1. Walters, E. A., and H. E. Nuttall, Potential for Underground Coal Gasification in the Southwest, published in the proceedings, ACS-Montreal, June 1977.

2. Nuttall, H. E., and E. A. Walters, In Situ Gasification of New Mexico's Deep Seam Coal Deposits via Nonmining Techniques, Technical Report, NE-37(77)BEF-363-1, April 1977.

3. Nuttall, H. E., and C. Anderson, A Field and Laboratory Project to Assess the Technical Suitability of New Mexico's Deep Seam San Juan Coal for In Situ Coal Gasification, proceedings of the 4th Underground Coal Conversion Symposium, Steamboat Springs, CO, July 17-20, 1978.

4. Nuttall, H. E., and F. L. Williams, Fossil Energy Research at the University of New Mexico, submitted for publication to the New Mexico Society of Professional Engineers, March 1979.

5. Stone, W. J., and N. H. Mizell, Basic Subsurface Data Compiled for Hydrogeologic Study of the San Juan Basin, Northwest New Mexico, Open-File Report 89, New Mexico Bureau of Mines & Mineral Resources, December 1978.